Development of early postnatal inhibitory function in the mouse medial prefrontal and primary somatosensory cortex

Katerina Kalemaki[1,2], Xiaxia Xu[3], Angeliki Velli[2,4], Ourania Christodoulou[4,5], Myrto Denaxa[5] Ileana L. Hanganu-Opatz[3], Domna Karagogeos[1, 2*] and Kyriaki Sidiropoulou[2,4*]

[1]Department of Basic Science, Faculty of Medicine, University of Crete, Heraklion, Greece

[2]Institute of Molecular Biology and Biotechnology (IMBB), FORTH, Heraklion, Greece

[3]Developmental Neurophysiology, Institute of Neuroanatomy, University Medical Center Hamburg-Eppendorf, Hamburg, Germany

[4]Department of Biology, University of Crete, Heraklion, Greece

[5]BSRC 'Alexander Fleming'

[*] co-corresponding author and equal senior contribution

Abstract

The prefrontal cortex (PFC) is characterized by protracted maturation that extends until adulthood. The cellular mechanisms controlling the early development of prefrontal circuits are still largely unknown. Our study delineates the developmental cellular processes that are on-going in the mouse medial PFC (mPFC) during the second and third postnatal weeks and compares them to those in the barrel cortex (BC). We show that basal synaptic transmission decreases from the second to the third postnatal week in both brain areas due to increased spontaneous inhibitory currents and reduced excitatory ones. Moreover, the GABAergic interneurons in the neonatal mPFC exhibit immature active properties. Furthermore, increasing $GABA_A$ receptor ($GABA_AR$) activity leads to increased basal synaptic response and spontaneous activity of neonatal mPFC, but not BC. Additionally, the K-Cl co-transporter 2 (KCC2) expression is decreased in the neonatal mPFC compared to the pre-juvenile one as well as to the neonatal and pre-juvenile BC, suggesting that $GABA_AR$ function in the neonatal mPFC is depolarizing. Therefore, our study reveals two significant differences in the maturation of GABAergic function of mPFC compared to BC: a developmental delay in the depolarizing function of GABA and the immature active properties of GABAergic interneurons.

Abbreviations

BC: Barrel Cortex

mPFC: medial Prefrontal Cortex

P10: Postnatal day 10

PNs: Pyramidal neurons

INs: Interneurons

Introduction

During early postnatal development, major events that contribute to cortical circuit maturation include spatial and temporal patterns of electrical activity, intrinsically determined cell death of early postnatal cortical interneurons and the depolarizing action of the neurotransmitter GABA (γ-aminobutyric acid) (Khazipov et al. 2004; Khazipov and Luhmann 2006; Allene et al. 2008; Brockmann et al. 2011; Ben-Ari et al. 2012; Southwell et al. 2012; Khazipov et al. 2013; Kirmse et al. 2015; Mòdol et al. 2019). The developmental switch of GABA action from depolarizing to hyperpolarizing results from changes in chloride co-transporter expression: Na^+-K^+-Cl^- cotransporter 1 (NKCC1), the Cl^- importer, is highly expressed early in development, while the expression of the co-transporter KCC2, the Cl^- exporter, increases after the first postnatal week (Ben-Ari 2001; 2002; Ben-Ari et al. 2007; Ben-Ari 2012). In addition, both intrinsic properties of neurons and synaptic transmission undergo dramatic changes during early postnatal development in a brain-area specific manner (Kriegstein et al. 1987; McCormick and Prince 1987; Burgard and Hablitz 1993; Ramoa and McCormick 1994; Bahrey and Moody 2003). Most studies on these developmental changes of the GABAergic system in the cortex have focused on the primary somatosensory cortex, visual cortex and hippocampus (Bartolini et al. 2013; Le Magueresse and Monyer 2013; Hensch 2016). The barrel cortex (BC) is part of the primary somatosensory cortex and is organized vertically in columns of cells associated with sensory perception (Guo et al. 2014) and horizontally in six layers of distinct cell types. In contrast, cortical association areas such as the prefrontal cortex (PFC) regulate cognitive functions and do not directly control sensory information (Fuster 2015). Anatomically, the mouse medial PFC (mPFC) is defined as the agranular part of frontal lobe, lacking the prominent granular layer IV and is divided into distinct subregions, namely infralimbic, prelimbic and cingulate cortex (Heidbreder and Groenewegen 2003; Van De Werd et al. 2010). The timeline of

mPFC development is delayed compared to other sensory cortices, such as BC (Casey et al. 2000; Best and Miller 2010; Kolb et al. 2012). From infancy to adulthood, the developing mPFC undergoes considerable transcriptional, structural and functional changes (Diamond 2005; Tsujimoto 2008; Kolb et al. 2012; Schubert et al. 2014; Kroeze et al. 2017).

While adolescent development of prefrontal circuitry and the underlying cellular mechanisms have been addressed by a large number of studies, only few investigations tackled the wiring processes at earlier stages (Brockmann et al. 2011; Bitzenhofer et al. 2015; 2017). However, specific knowledge is missing for the physiological and cellular changes that are on-going in the mPFC between the second (neonatal) and third (pre-juvenile) postnatal week. Here, we aim to fill this gap by investigating the synaptic and intrinsic properties of neonatal and pre-juvenile mPFC neurons and comparing them to those in the BC, with a primary focus on the GABAergic system.

Methods

All *in vitro* experiments with mice took place under an experimental protocol approved by the Research Ethics Committee and by our Institutional Animal Care and Use Committee that has been approved by the Veterinarian Authorities Office (protocol license no. 93164). Experiments were carried out by trained scientists and in accordance with the 3R principles. *In vivo* experiments were performed in compliance with the German laws and the guidelines of the European Community for the use of animals in research and were approved by the local ethical committee (015/17, 015/18).

Animals

The *in vitro* experiments were performed on male C57Bl/6J; Lhx6Tg(Cre); R26R-YFP+/+ mice from animal facility of IMBB-FORTH were used. For the *in vivo* experiments, timed-pregnant C57BL/6J mice from the animal facility of the University Medical Center Hamburg-Eppendorf were used. The day of vaginal plug detection was defined as embryonic day (E)0.5, whereas the day of birth was defined as P0. The offspring of both sexes are used for *in vivo* electrophysiology recordings. All procedures were performed according to the European Union ethical standards outlined in the Council Directive 2010/63EU of the European Parliament on the protection of animals used for scientific purposes.

Mice were housed with their mothers and provided with standard mouse chow and water ad libitum, under a 12 h light/dark cycle (light on at 7:00 am) with controlled temperature (21°C). The P10 experimental group includes ages P9-P11 and the P20 group includes ages P19-P21, also referred to as second and third postnatal weeks or neonatal and pre-juvenile, respectively. All efforts were made to minimize both the suffering and the number of animals used.

In vitro extracellular recordings

Slice Preparation*:* Mice (P10 and P20) were decapitated under halothane anesthesia. The brain was removed promptly and placed in ice cold, oxygenated (95% O_2 –5% CO_2) artificial cerebrospinal fluid (aCSF) containing (in mM): 125 NaCl, 3.5 KCl, 26 $NaHCO_3$, 1 $MgCl_2$ and 10 glucose (pH = 7.4, 315 mOsm/l). The brain was blocked and glued onto the stage of a vibratome (Leica, VT1000S). Rostrocaudal coronal slices (400 µm thick) containing either the mPFC (prefrontal cortex) or the BC (barrel cortex) region were selected and transferred to a submerged chamber, which was continuously superfused with oxygenated (95% O_2 –5% CO_2) aCSF containing (in mM): 125 NaCl, 3.5 KCl, 26 $NaHCO_3$, 2 $CaCl_2$, 1 $MgCl_2$ and 10 glucose (pH = 7.4, 315 mOsm/l) at room temperature (RT). The slices were allowed to equilibrate for at least 1 h in this chamber before recordings began. Slices were then transferred to a submerged recording chamber, continuously superfused with oxygenated (95% O_2 –5% CO_2) aCSF (same constitution as the one used for maintenance of brain slices) at RT during recordings.

Data Acquisition: Electrophysiological recordings were performed in all experimental groups under the same conditions as described below. Pulled glass micropipettes were filled with NaCl (2M) and placed in layers II/III of PFC and BC. Platinum/iridium metal microelectrodes (Harvard apparatus United Kingdom, 161 Cambridge, United Kingdom) were placed on layer II/III of the mPFC and the BC, about 300 µm away from the 1MΩ recording electrode, and were used to evoke field excitatory postsynaptic potentials (fEPSPs). Local field potentials (LFPs) were amplified using a headstage with selectable high pass filter of 30 Hz to remove any offsets coupled to a Dagan BVC-700A amplifier, amplified 100 times and low-pass filtered at 1-kHz. A notch filter was used to eliminate line frequency noise at 30 Hz. Signals were digitized using the ITC-18 board (InstruTech, Inc.) on a PC with custom-made procedures in IgorPro (Wavemetrics, Inc.) and stored on a PC hard drive. All voltage signals were collected at a sampling frequency of 100 kHz (fs = 100 kHz).

For evoked fEPSPs, the electrical stimulus consisted of a single square waveform of 100 μs duration given at intensities of 0.1– 0.3 mA (current was increased from 0.1 mA to 0.3 mA, with 0.1 mA steps) generated by a stimulator equipped with a stimulus isolation unit (World Precision Instruments, Inc.). The effect of $GABA_AR$ activation was investigated by bath application of 2 μM Diazepam ($GABA_AR$ agonist). Diazepam was acquired from the Pharmacy of the University General Hospital in Heraklion as a 5 mg/ml solution and was diluted in aCSF during recordings. Other drugs used include CNQX (10μM), AP5 (50μM) and bumetanide (10μM) (Tocris). For spontaneous activity recordings, 20 5-sec recordings were acquired without any stimulation.

Data Analysis: Data were analyzed using custom-written procedures in IgorPro software (Wavemetrics, Inc.). No additional high-pass filters were applied to the raw data. For evoked recordings, the peak values of the fEPSP were measured using the minimum value of the synaptic response (4–5 ms following stimulation) and were compared to the baseline value prior to stimulation. Both parameters were monitored in real- time in every experiment. A stimulus–response curve was then plotted using stimulation intensities between 0.1 and 0.8 mA, in 0.1 mA steps. For each different intensity level, two traces were acquired and averaged.

To identify spontaneous activity events, the acquired spontaneous activity voltage signals of 5 seconds' duration were decimated (down-sampled) by a factor of 10 and the standard deviation σ_b of background signal was calculated in the 'quiet' part of each voltage response trace. To identify the 'quiet' period, each 5sec trace was split into 100msec increments and the range of voltage deflection was computed in each increment. The 'quiet' part of the LFP trace was the 100msec increment with the smallest σ_b value. As a spontaneous event, any voltage response larger than $4 \cdot \sigma_b$ was identified. We calculated the frequency of spontaneous events by measuring the number of spontaneous events divided by the duration of the trace (5s). The frequency was calculated in 20 consecutive 5-sec traces and then averaged for each condition animal. The spontaneous events do not correspond to spiking of individual neurons, they rather reflect population spikes.

In vitro **patch-clamp recordings**

Slice Preparation: Mice were decapitated under halothane anesthesia. The brain was removed immediately and coronal slices of mPFC and BC (300–350 μm thick), using a vibratome (Leica, VT1000S, Leica Biosystems) were prepared from mice at the ages of P10 and P20 in ice-cold oxygenated (95% O_2 - 5% CO_2) modified choline-based aCSF (in mM) 0.5 $CaCl_2$, 7 mM $MgSO_4$;

NaCl replaced by an equimolar concentration of choline). Slices were incubated for 30min at 32°C in an oxygenated normal aCSF containing (in mM): 126 NaCl, 3.5 KCl, 1.2 NaH_2PO_4, 26 $NaHCO_3$, 1.3 $MgCl_2$, 2.0 $CaCl_2$, and 10 D-glucose, pH 7.4, 315 mOsm/l. Slices were allowed to equilibrate for at least 30 min at RT before being transferred to the recording chamber. During recordings, slices were perfused at a rate of 4 ml/min with continuously aerated (95% O_2-5% CO_2) normal aCSF at RT.

Data Acquisition: Neurons were impaled with patch pipettes (5–7 MΩ) and recorded in the whole-cell configuration, either in the current-clamp or voltage-clamp mode. For current-clamp experiments, the composition of the intracellular solution was: 130 mM K-$MeSO_4$, 5 mM KCl, 5 mM NaCl, 10 mM HEPES, 2.5 mM Mg-ATP, and 0.3 mM GTP, 265–275 mOsm, pH 7.3. For voltage-clamp experiments, the composition of the intracellular solution was: 120 mM Cs-gluconate, 20mM CsCl, 0.1 mM $CaCl_2$, 1 mM EGTA, 0.4 mM Na-guanosine triphosphate, 2mM Mg-adenosine triphosphate, 10 mM HEPES. No correction from liquid junction potential was applied between the pipette and the aCSF. Whole-cell measurements were low-pass filtered at 5 kHz using an Axopatch 200B amplifier (Molecular Devices, Inc). Recordings were digitized with the ITC-18 board (Instrutech, Inc) on a PC using custom-made codes in IgorPro (Wavemetrics, Inc). All signals were collected at a sampling frequency of 20kHz.

Data Analysis: Data were analyzed using custom-written codes in IgorPro software (Wavemetrics, Inc.). For passive membrane properties, the resting membrane potential (RMP, mV) was measured within 3 min after establishing the whole-cell configuration, and monitored throughout the experiment. To measure input resistance, a 500ms step-pulse protocol was used with current stimulation from -200pA to +50pA. The input resistance (R_{in}, MΩ) was measured by plotting the steady-state voltage deflection in an I-V plot and calculating the slope of the best fit line curve (R_{in}=V/I). The τ_m (membrane time constant, ms) was obtained by fitting a single exponential curve to the voltage deflection at -50pA, and the membrane capacitance (C_m) was calculated using the formula $C_m = \tau_m/R_{in}$. In addition, the number of spikes generated in response to a 500ms step-pulse range from +100pA to +300pA was measured.

To measure action potentials (APs) properties, we applied small supra-threshold 5ms step-pulse currents to the cell from -65mV. The active properties were measured at the minimum current stimulation (Rheobase, pA) that generated an AP. The AP threshold (mV) was calculated by taking the first derivative of the voltage trace, defining a threshold and identifying the voltage level at that time point. The rate of rise of the AP (dV/dt, mV/ms) was the maximum value of

that first derivative trace. The AP amplitude (mV) was defined as the voltage difference between AP threshold and AP peak. The AP duration (ms) was calculated by the full width of the waveform at the half maximal amplitude (half-width). The fast afterhyperpolarization (fAHP) minimum (mV) was defined as the minimum voltage right after the AP. The fAHP amplitude (mV) was calculated as the difference between the AHP minimum and the AP threshold. The fAHP time (ms) was defined as the time duration from the time point of AP threshold to the fAHP minimum. The composition of our intracellular solution resulted in chloride reversal potential of -60mV and Na^+/K^+ reversal potential of +10mV. This allowed for measurements of spontaneous excitatory postsynaptic currents (sEPSCs) to be recorded at -60mV and of spontaneous inhibitory postsynaptic currents (sIPSCs) to be recorded at +10mV. Automatically selected events were subsequently visually monitored to discard erroneously included noise. The events showing only single peaks were selected for kinetics analysis. All currents detected from every single neuron were averaged. The peak amplitude was calculated as the maximum current value. The time constant of the decay phase was detected by curve fitting with a single exponential decay function.

***In vivo* extracellular recordings**

Surgery: Multisite extracellular recordings were performed in the PFC of P8–P10 (n=13) and P20–P23 (n=14) C57/BL mice with both sexes. Mice were under urethane anesthesia (intraperitoneal injection, 1 mg/g body weight; Sigma-Aldrich) before surgery. The bone over the mPFC (0.8 mm anterior to bregma, 0.1–0.5 mm right to the midline) was carefully removed. One-shank electrodes with 4 recording sites (0.4–0.8 MΩ impedance, 100 µm spacing, NeuroNexus) was inserted into PFC at a depth of 1.9 mm from the skull surface. Electrodes were labelled with DiI (1,1'-dioctadecyl-3,3,3',3'-tetramethyl indocarbocyanine; Invitrogen) to confirm their position after histological assessment post-mortem. One silver wire was inserted into the cerebellum to serve as ground and reference electrode.

Data Acquisition: A recovery period of 10 min following the insertion of electrodes before acquisition of data was provided. Data acquired during the first 30 min of recording were used for analysis to ensure similar state of anesthesia in all investigated pups. Extracellular signals were bandpass filtered (0.1 Hz to 5 kHz) and digitized (32 kHz) with a multichannel extracellular amplifier (Digital Lynx SX, Neuralynx) and the Cheetah acquisition software (Neuralynx).

Data Analysis: Data were imported and analyzed off-line using custom-written tools in MATLAB software version 7.7 (MathWorks). Multiple unit activity (MUA) is detected when negative deflections exceeding five times the SD of the bandpass filtered (500–5000 Hz) signals. Single unit activity (SUA). SUA was detected and clustered using klusta (Rossant et al., 2016) and manually curated using phy (https://github.com/cortex-lab/phy). Data were imported and analyzed using custom-written tools in the MATLAB. Burst activity detection. Burst activity was detected by using the method from (Gorin, Tsitoura et al. 2016). First, for each unit, Poisson distribution, which assumed random independent spiking, was defined. The single parameter λ of Poisson distribution is the average firing rate of the unit. Second, the median ISI value of the Poisson distribution was derived. Third, we defined a burst activity as a sequence of ≥4 consecutive spikes separated by intervals smaller than the median ISI. Last, the percentage of the burst activity of a single unit is calculated by 100* (the number of the burst activity / the number of the spikes). A unit was classified as "burst unit" if >50% of all spikes occurred in bursts.

Immunohistochemistry

Mice at the age of P10 and P20 were perfused with 4% paraformaldehyde, followed by fixation with the same solution for 1h at 4◦C, followed by cryoprotection and preparation of 12 µm cryostat sections as previously described[88]. Primary antibodies used were rat monoclonal anti-GFP (Nacalai Tesque, Kyoto, Japan, 1:5000), rabbit polyclonal anti-GFP (1:500; Minotech biotechnology, Heraklion, Greece) and rabbit polyclonal anti- parvalbumin (PV) (Swant, Bellinzona, Switzerland; 1:2000. Secondary antibodies used were goat anti-rat-Alexa Fluor-488, goat anti-rabbit Alexa Fluor-488, and goat anti-rabbit-Alexa Fluor-555 (Molecular Probes, Eugene, OR, United States, 1:800). Images were obtained with a confocal microscope (Leica TCS SP2, Leica, Nussloch, Germany). For each age group (P10, P20), 2-4 10µm-thick sections from each mouse brain were selected, all including the mPFC and BC.

RNA *In Situ* Hybridization

Non-radioactive *in situ* hybridization experiments were performed on cryostat sections (12µm thick, see immunochemistry) according to the protocol described (Schaeren-Wiemers and Gerfin-Moser 1993). Riboprobe was prepared by *in vitro* transcription and was specific Somatostatin (SST) (Liodis et al. 2007).

Nissl Staining

Cryostat sections (12µm thick, see immunochemistry) were incubated in 1:1 100% ethanol:chloroform overnight at RT. Then, sections were rehydrated for 1 min in 100%, 95% ethanol solutions and dH_2O at RT, followed by a 10-min incubation in 0.1% cresyl violet solution at 50°C. Sections were then dehydrated with dH_2O, 95%, 100% ethanol and xylene for 5 min and coverslipped with permount. Images from whole sections were obtained in 5× magnification of a light microscope (Axioskop 2FS, Carl Zeiss AG, 268 Oberkochen, Germany) and merged using Adobe Photoshop CC 2015, Adobe Systems, Inc.

Analysis for Immunochemistry, *in situ* hybridization and Nissl staining

The background color of each cropped image was converted to black, while the cells were colored blue. The images were loaded into Matlab, where the number of 'blue' pixels was counted per area (mm^2). Each cell was assumed to be composed of four pixels. Therefore, the number of cells was measured as the total number of 'blue' pixels divided by four (Konstantoudaki et al. 2016; Chalkiadaki et, 2019). The results of the algorithm were double checked with hand counting first, before applying the algorithm to multiple slices. An average number was calculated for the number of neurons from mPFC and BC sections from each developmental group.

Western blots

Mice were decapitated following cervical dislocation, the brain was quickly removed, placed in ice cold PBS (phosphate-buffered saline) and then positioned on a brain mould, where 1.5 mm slices were taken containing the mPFC and BC. The slices were placed on dry ice, and the prelimbic area of mPFC was dissected out and stored at -80°C. The BC was also isolated from the corresponding slices and stored at -80°C. Frozen tissue blocks were lysed in a solution containing (in mM) HEPES 50, NaCl 150, MgCl2 1.5, EGTA 5, Glycerol 1%, Triton-X100 1%, 1:1000 protease inhibitors cocktail. Proteins ran on 8.5% bis-acrylamide gel and were transferred onto a nitrocellulose membrane (Whatman GmbH, Dassel, Germany). The membrane was blocked, incubated in rabbit polyclonal anti-K+/Cl-Cotransporter (KCC2) (Merck KGaA, Darmstadt, Germany, 1:1000) or rabbit monoclonal anti-GAPDH (Cell Signaling Technology Europe BV, Leiden, Netherlands, 1:1000), washed, incubated in secondary goat anti-rabbit IgG Horseradish Peroxidase Conjugate antibody (Invitrogen, 1:5000), and digitally exposed using the Molecular

Imaging system ChemiDoc (BioRad Laboratories, Inc, California, U.S.A.). Analysis of KCC2 and GAPDH expression was performed with ImageJ software, and the raw values of KCC2 from each sample were normalized to their respective GAPDH values.

Statistical analysis

Statistical analyses were performed in Microsoft Office Excel 2007 and GraphPad Prism Software 7.0. Data are presented as mean ± standard error of mean (SEM). Normality distribution and equality of variances of dataset were tested with the Kolmogorov-Smirnov test normality test. The null hypothesis was rejected for a >5%. When four experimental groups (P10 mPFC, P20 mPFC, P10 BC and P20 BC) were assessed and two variables were taken into consideration (age and brain area), data were analyzed with a two-way ANOVA with Fisher LSD, Sidak's or Tukey's multiple comparisons (electrophysiological recordings and cell counting). When three groups (P10 mPFC, P20 mPFC and P10 BC) data were analyzed with one- way ANOVA (electrophysiological recordings). For the comparison of *in vivo* spiking activity between P10 and P20, statistical analyses were performed with MATLAB. Significant differences were detected by one-way ANOVA. Significance levels of *p < 0.05, **p < 0.01, ***p < 0.001 or ****p < 0.0001 were tested. For comparison of Western blot analysis, the significant effect of each developmental age group from mPFC and BC was assessed using Student's t-test depending on the experiment.

Data availability

Data presented in the figures in this paper are available upon request.

Results

Mice belonging to two age groups were investigated: (i) neonatal mice included pups of postnatal days (P) 9-11 and are defined as P10 while (ii) pre-juvenile mice defined as P20 animals including pups of P19-P21. Due to the high density of intra-cortical synapses in the superficial cortical layers (DeFelipe and Fariñas 1992; Clancy et al. 2001) and their specific involvement in neurodevelopmental disorders (Chini and Hanganu-Opatz, 2020; Bitzenhofer eta l., 2017) we focused on the superficial layers of the mPFC and BC. From each mouse brain, both the mPFC and the BC were studied. All analyses that had four groups (mPFC P10 and P20, BC P10 and P20)

were conducted using two-way ANOVA, with the two factors being the brain area (mPFC and BC) and age (P10 and P20).

Synaptic transmission decreased in mPFC and BC across development

First, we investigated the synaptic properties of mPFC and BC in neonatal compared to juvenile mice. We measured basal synaptic transmission using extracellular field recordings in brain slices. The evoked field excitatory postsynaptic potentials (fEPSPs) in layer II/III of both areas were recorded in response to current pulses of increasing intensity through the stimulating electrodes in layer II/III (**Figure 1a,c**). The fEPSPs were significantly decreased in both mPFC and BC at P20 compared to P10 (**Figure 1b,d**).

The decreased fEPSP responses at P20, compared to P10 (**Figure 1b,d**), could result from either increased inhibitory postsynaptic currents or decreased excitatory postsynaptic currents. To examine this, we performed patch-clamp recordings from layer II/III pyramidal neurons in mPFC and BC from P10 and P20 mice. We recorded spontaneous inhibitory postsynaptic currents (sIPSCs, at +10mV) and spontaneous excitatory postsynaptic currents (sEPSCs, at -60mV) and we measured the frequency, amplitude and decay time constant.

In mPFC, the frequency of sIPSCs was significantly augmented at P20 compared to P10 (**Figure 2a,b**), while the sIPSC amplitude and decay-time constant did not significantly change over the investigated time window (**Figure 2a,c,d**). The sIPSC frequency remained increased at P20, compared to P10, in the presence of AMPA and NMDA receptor antagonists, CNQX and AP5, respectively. On the other hand, bicuculine, a $GABA_A$ receptor antagonist, blocked the sIPSCs both in P10 and P20 mPFC (Supplemental Figure 1). In BC, sIPSC frequency and amplitude were significantly increased, at P20 compared to P10 (**Figure 2a,b,c**), while the decay-time constant was not altered (**Figure 2a,d**). When comparing the two brain areas, we noticed a significantly lower sIPSC frequency in the mPFC compared to BC at both ages (**Figure 2a,b**). The decay time constant was similar (**Figure 2a,d**), while the sIPSC amplitude was significantly smaller at P20 in the mPFC compared to BC (**Figure 2a,c**).

The sEPSC frequency was significantly decreased at P20 compared to P10, in both areas (**Figure 2e,f**), while the amplitude and decay time constant were unaltered (**Figure 2e,g,h**). However, in the presence of bicuculine (10uM) the sEPSC frequency was reduced at mPFC P10 and was not different between P20 and P10 mPFC (Supplemental Figure 1). Upon comparing the two brain areas, the sEPSC frequency and amplitude were found significantly decreased in mPFC,

compared to BC, at P10 (**Figure 2e,f**). At P20, the sEPSC frequency was similar between the two cortical areas, while the amplitude remained significantly smaller in mPFC compared to BC in both ages (**Figure 2e,g**). The decay time constant was not different between areas at both ages (**Figure 2e, h**).

The increased sIPSC frequency can underlie the fEPSP reduction from P10 to P20 in mPFC and BC (**Figure 1b,d**). In addition, specifically for mPFC, the possibility for the presence of $GABA_A$-mediated sEPSCs could also contribute to the fEPSP reduction from P10 to P20.

Passive and active membrane properties of MGE-derived interneurons are altered in the mPFC across development

Changes in interneuron properties could underlie the increased sIPSC frequency. To investigate this, we performed current-clamp recordings from layer II/III mPFC and BC of $Lhx6^+$ interneurons. For this reason, Lhx6-cre;ROSA26fl-STOP-fl-YFP mice were used in which $Lhx6^+$ interneurons express YFP. Lhx6 is expressed by all post-mitotic and mature MGE-derived interneurons (Liodis et al. 2007), therefore, YFP is expressed in MGE-derived interneurons, which include interneurons that express parvalbumin (PV^+) and somatostatin (SST^+).

Upon analysis of the passive properties, we found a significant increase in the input resistance and membrane time constant, as well as a significant decrease in the membrane capacitance in the mPFC at P10 compared to P20. In addition, the input resistance and the membrane time constant were higher at P10 mPFC, compared to BC (P10 and P20). There was no difference in the resting membrane potential (RMP) between ages and brain areas (**Figure 3, Supplementary Table 1**).

With regard to the active properties, there was no significant difference between ages and brain areas in the AP amplitude, AP threshold, rheobase and fAHP time (Figure 4a, d, e, g; **Supplementary Table 1**). The AP rate of rise (dv/dt) was significantly increased while the AP duration (half-width) was significantly reduced at P20 compared to P10 in both the mPFC and BC (**Figure 4b-c, Supplementary Table 1**). In addition, the fAHP amplitude was significantly lower in the mPFC (**Figure 4f, Supplementary Table 1**), compared to BC. The increased rate of rise and the decreased AP duration are possibly linked with the up-regulation of voltage-dependent sodium channels during development (Huguenard et al. 1988), and in combination with the reduced fAHP amplitude suggest that the mPFC MGE-interneurons at P10 are still quite

379 immature, when compared to adult PV^+/SST^+ interneurons in mPFC (Yang et al. 2013; Pan et al.
380 2017).
381 Overall, these data indicate that some intrinsic properties of interneurons in mPFC change with
382 age (from P10 to P20), reaching values that closer resemble adult MGE-derived interneurons
383 (Yang et al. 2013; Pan et al. 2017). Therefore, the increased sIPSC frequency of mPFC pyramidal
384 neurons observed at P20, compared to P10 could partly be explained by these altered properties
385 of presynaptic interneurons.
386
387 **The emergence of PV immunoreactivity is delayed in mPFC compared to BC**
388 An additional explanation for the increased sIPSC frequency could come from alterations in
389 interneuron cell densities. To test this, we quantified the number of interneurons per area in
390 cryosections at P10 and P20 mPFC and BC coronal brain slices of $Lhx6^+$-expressing mice. The YFP^+
391 positive cells per area (i.e. $Lhx6^+$ cell density) in mPFC and BC was similar between ages, but was
392 significantly lower in the mPFC, compared to BC (**Figure 5a**). The percentage of cell death in
393 $Lhx6^+$ neurons is very low in both P10 mPFC and BC (**Supplementary Figure 2**).
394 The transcription factor Lhx6 is required for the specification and maintenance of main MGE-
395 derived interneurons, PV and SST-positive interneuron subtypes, at postnatal ages (Liodis et al.
396 2007). The neuropeptide SST (both mRNA and protein) is progressively expressed from
397 embryonic to postnatal levels (Bendotti et al. 1990; Forloni et al. 1990). We found that the SST
398 mRNA levels were similar between areas and ages (**Figure 5b**). On the other hand, the
399 emergence of PV immunoreactivity in the mouse cortex shows a delayed development, starting
400 from early postnatal period to adult, with marked area-specific differences(Del Rio et al. 1992).
401 We found that PV was only immunoreactive in BC, and not in mPFC, at P10 (**Figure 5c and**
402 **Supplementary Figure 3 and 4**). At P20, PV was immunoreactive in both mPFC and BC, but PV^+
403 cell density was significantly lower in the mPFC, compared to BC (**Figure 5c and Supplementary**
404 **Figure 3 and 4**).
405 We also counted the total cell density of mPFC and BC from neonatal and juvenile mice
406 (**Supplementary Figure 5a**) using Nissl staining. In the mPFC, the cell density significantly
407 decreased at P20 compared to P10 (**Supplementary Figure 5b**). On the contrary, in BC, the total
408 cell density significantly increased at P20 compared to P10 (**Supplementary Figure 5b**). When
409 the two brain areas were compared, no difference was found at P10, while the mPFC cell density
410 was significantly lower compared to BC at P20 (**Supplementary Figure 5b**).

We further examined whether the alterations in total cell density are derived from alterations in cell density of interneurons by measuring the $Lhx6^+$ neurons over the Nissl-positive cells. No differences were detected between areas and ages (**Supplementary Figure 5c).** These results suggest that the changes in total cell density in mPFC and BC respectively are probably due to changes in other neuronal or glial populations.

GABA is depolarizing in the neonatal mPFC but not BC

Our data so points at several similarities in the development of mPFC and BC from the neonatal to pre-juvenile period, but also indicates a protracted maturation of several mPFC interneuron properties (intrinsic properties and PV immunoreactivity). Therefore, it is likely that another GABAergic developmental process occurs at a later time point in the mPFC, and specifically, that of the switch from depolarizing to hyperpolarizing function of $GABA_AR$. It is well known that $GABA_AR$ is depolarizing during the first postnatal week, but switches to hyperpolarizing at P7 in the hippocampus, cortex and amygdala (Ben-Ari et al. 1989; Luhmann and Prince 1991; LoTurco et al. 1995; Owens et al. 1996; Martina et al. 2001; Gulledge and Stuart 2003; Ben-Ari et al. 2007; Kirmse et al. 2015). Therefore, at P10, $GABA_AR$ function is inhibitory in the BC. We used diazepam (2µM) (a $GABA_AR$ agonist) to enhance $GABA_AR$ function and determine whether it is depolarizing by measuring the fEPSP response. At P10, diazepam did not significantly alter the fEPSP in BC, as expected if $GABA_AR$ function is inhibitory. However, diazepam increased the fEPSP amplitude in mPFC at P10 (**Figure 6a-b**). At P20, the fEPSP amplitude was not significantly altered following diazepam application in both mPFC and BC (**Figure 6c,d**). The fEPSP enhancement was also evident in the presence of AMPA and NMDA receptor antagonists (CNQX and AP5) (Supplementary Figure 6a-c). These results suggest that the $GABA_AR$ function is depolarizing in the mPFC at P10.

The switch in the $GABA_AR$ function from depolarizing to hyperpolarizing occurs due to the increased expression of the K^+-Cl^- co-transporter 2 (KCC2) (Rivera et al. 1999). To determine whether modulating chloride transporters could alter the diazepam-induced enhancement of the fEPSP, we recorded the fEPSP in the presence of bumetanide (10uM), which blocks the NKCC1 transporter, and tested the effect of diazepam. We find that in the presence of bumetanide, diazepam did not result in an increase of the fEPSP (Supplementary Figure 6). In addition, we measured KCC2 protein levels and demonstrated that they were significantly increased at P20 compared to P10 in the mPFC but not in the BC (**Figure 7a,b**). These results

443 further support our hypothesis that the $GABA_AR$ function is depolarizing at P10 in the mPFC and
444 could explain the observed increased fEPSPs, sEPSC frequency and decreased sIPSCs.
445
446 **No significant changes in pyramidal neuron excitability**
447 To determine whether the reduced sEPSC frequency can be explained by changes in pyramidal
448 neuron excitability, we investigated their intrinsic properties. The passive and active properties
449 of these neurons were measured using current-clamp recordings from layer II/III mPFC and BC
450 pyramidal neurons. With regards to passive properties, no significant differences were observed
451 in the RMP, the input resistance and the membrane time constant between brain regions and
452 ages (**Supplementary Figure 7, Supplementary Table 1**). Only the membrane capacitance was
453 significantly increased at P20 compared to P10 (**Supplementary Figure 7d, Supplementary Table**
454 **1**), in both brain areas. In addition, the number of spikes generated with increasing current
455 stimulation was not significantly different between ages and regions (**Supplementary Figure 8**).
456 In terms of active properties, the AP amplitude and rate of rise were increased at P20 compared
457 to P10 mPFC, while the AP half-width, rheobase and threshold were not significantly different
458 (**Figure 8, Supplementary Table 1**). The AP amplitude was also significantly increased at P20,
459 compared to P10 in BC, while the other properties did not change (**Figure 8, Supplementary**
460 **Table 1**). Comparing the two regions at the two ages, we found no significant differences of AP
461 properties of pyramidal neurons (**Figure 8, Supplementary Table 1**). The developmental increase
462 of AP amplitude and rate of rise in the mPFC could be due to the on-going maturation of sodium
463 channels in pyramidal neurons. However, these changes could not account for the reduced
464 sEPSCs in the neonatal, compared to pre-juvenile, mPFC and BC.
465
466 **Diazepam-modulated spontaneous activity in mPFC brain slices of neonatal mice**
467 To understand how network activity is affected in the neonatal mPFC compared to the juvenile
468 mPFC, we initially recorded spontaneous activity in mPFC brain slices. We find that spontaneous
469 activity events are significantly increased in the juvenile mPFC compared to the neonatal mPFC
470 (Figure 9a,b). On the other hand, there is no difference in the number of spontaneous activity
471 events between P10 and P20 in the BC (Figure 9a,b). Furthermore, the addition of diazepam
472 increased the number of spontaneous activity events by 100% compared to control conditions
473 at P10 in the mPFC (Figure 9Cc,d). The diazepam-induced change was significantly less at P20
474 mPFC, compared to P10 (Figure 9c,d). The concurrent administration of bumetanide (antagonist

of sodium-potassium-chloride (Na-K-Cl) cotransporters, NKCC1) and diazepam actually reduced the number of spontaneous events at P10 mPFC (50% less). This percent change was significantly less compared to the % change at P20 mPFC (Figure 9). We suggest that the spontaneous activity of early mPFC networks (P10) modulated by the excitatory action of $GABA_A$ R in combination with (Na-K-Cl) cotransporters.

Increased firing activity *in vivo* in the mPFC between the second and third postnatal weeks

To investigate the physiological network activity *in vivo*, multisite recordings of the LFP and multi-unit activity (MUA) were performed in layers II/III of mPFC at P8-10 and P20-23. A significant increase of MUA was identified at P22 compared to P9 mice, indicating a developmental increased spiking activity in layers II/III of mPFC on the third compared to the second postnatal week (Figure 10). Similarly, the spiking activity in the BC augmented with age (Supplementary Figure 9). To characterize the firing dynamics along development, we used MUA for clustering single-unit activity. We detected bursts of spikes using the previously developed method (Gorin et al. 2016). The burst occurrence in the mPFC increased with age (33.62±1.91 %, 161 single units at neonatal age vs. 50.12±4.91 %, 150 single units at pre-juvenile age; $p<0.0001$, One-way ANOVA, $F_{(1, 309)}=272.26$). Correspondingly, the number of units organized in bursts increased with age too from 21 out of 161 single units at neonatal age to 104 out of 150 single units at pre-juvenile age (Figure 10d). Moreover, we analyzed the mPFC and BC units in their amplitude, dv/dt and half-width and detected, similarly to the in vitro conditions, a significant increase in the AP amplitude and rate of rise but no difference in the half-width (Supplementary Figure 10). These results provide further evidence that the decreased excitatory synaptic activity of mPFC cannot be attributed to increased spiking activity of mPFC neurons at P10.

Discussion

Our study has identified significant developmental events in the mPFC and the BC between the second and third postnatal weeks. Specifically, we have shown that the basal synaptic transmission decreases from the second to the third postnatal week, a fact that can be explained by an increase in the sIPSCs in both mPFC and BC. Moreover, our data support a depolarizing action of $GABA_AR$ in the second postnatal week, in the mPFC only and not the BC, as indicated by the presence of non-AMPA-mediated sEPSCs, increased basal synaptic transmission following

507 $GABA_AR$ activation, which is blocked by concurrent bumetanide application, and decreased
508 protein levels of KCC2. In parallel, differences in the development of the intrinsic properties of
509 GABAergic interneurons from the neonatal to juvenile period were identified between the mPFC
510 and BC. Finally, the AP amplitude and AP rate-of-rise of pyramidal cells also change with age and
511 relate to augmented network activity across development, both *in vitro* and *in vivo*.
512
513 **Depolarizing action of GABA in the immature cortex**
514 GABA plays a crucial role in inhibiting adult neurons, acting primarily via the chloride-permeable
515 $GABA_AR$ and resulting in hyperpolarization of the membrane potential (Kaila and Voipio 1987).
516 However, GABA action leads to depolarization of immature neurons (i.e. during the first
517 postnatal week in mice), due to an initially higher intracellular chloride concentration $[Cl^-]_{in}$ (Ben-
518 Ari 2001; Ben-Ari et al. 2007; Ben-Ari 2012). The developmental switch of GABA action from
519 depolarizing to hyperpolarizing results from changes in cation-chloride co-transporter
520 expression: NKCC1, a cation-Cl^- importer, is highly expressed in neuronal precursor cells during
521 early brain development (Plotkin et al. 1997; Yamada et al. 2004), while the expression of the
522 K^+-Cl^- cotransporter 2 (KCC2), a cation-Cl^- exporter, increases after the first postnatal week (Ben-
523 Ari 2001; Ben-Ari et al. 2007; Ben-Ari 2012). This increased KCC2 transporter expression might
524 provide a central mechanism for the depolarization to hyperpolarization switch of GABAergic
525 transmission via progressive reduction of $[Cl^-]_{in}$ (Lu et al. 1999; Rivera et al. 1999; Ganguly et al.
526 2001; Ben-Ari 2002; Dzhala et al. 2005; Fiumelli et al. 2005).
527 The $GABA_AR$ switch from depolarizing to hyperpolarizing occurs at P7 in the hippocampus,
528 cortex, amygdala (Ben-Ari et al. 1989; Luhmann and Prince 1991; LoTurco et al. 1995; Owens et
529 al. 1996; Martina et al. 2001; Gulledge and Stuart 2003; Ben-Ari et al. 2007). Our study suggests
530 that this switch is delayed in the mPFC compared to primary somatosensory cortex and it takes
531 place between P10 and P20. Specifically, we show that increased $GABA_AR$ activity leads to
532 enhanced fEPSPs in neonatal mPFC (P10), suggesting that the $GABA_AR$ function is depolarizing in
533 the mPFC at P10. This enhancement is prevented in the presence of the NKCC1 blocker,
534 bumetanide. Furthermore, diazepam increases the number of spontaneous activity events in the
535 brain slice, which is also prevented in the presence of bumetanide. This hypothesis is further
536 supported by decreased levels of KCC2 transporter in the neonatal mPFC. Our results could have
537 implications for understanding the protracted maturation of mPFC compared to other cortical

538 areas, which may depend on a combination of a delayed switch from depolarizing-to-
539 hyperpolarizing function of $GABA_AR$ and maturation of interneurons.
540
541 **Interneurons and mPFC development**
542 Recordings of $Lhx6^+$- interneurons indicate that both passive and active properties are regulated
543 by age and reach values that better resemble adult MGE-derived interneurons. Specifically, we
544 have found that the input resistance and AP width decrease while the AP rate of rise increases
545 in the mPFC at P20 compared to P10. In part, similar findings have been identified for PV^+ cells
546 in the hippocampus (Doischer et al. 2008; Miyamae et al. 2017) and SST^+ cells in the anterior
547 cingulate cortex (Pan et al. 2017). On the other hand, the AHP amplitude is still quite immature
548 in the mPFC at P20, compared to PV^+, SST^+ interneurons in primary sensory areas or the
549 hippocampus and compared to adult mPFC (Doischer et al. 2008; Yang et al. 2013; Pan et al.
550 2017). Therefore, it is likely that the physiological properties of PV+ and SST+ interneurons in
551 the mPFC continue to change past the third postnatal week.
552 Our knowledge on the neonatal physiology of mPFC GABAergic interneurons is very limited. It
553 has been shown that PV expression is lowest in juveniles and increases during adolescence to
554 levels similar to those observed in adulthood (Caballero et al. 2014). Furthermore, PV expression
555 is not evident in the neonatal period and emerges during the pre-juvenile period in the mPFC
556 (del Rio et al. 1994; de Lecea et al. 1995; Zheng et al. 2011; Spampanato and Sullivan 2016). Our
557 results agree with these findings, as PV expression was detected in very low amounts during the
558 pre-juvenile period in the mPFC.
559 In addition, our study has identified decreased excitatory and increased inhibitory synaptic
560 function between the second and third postnatal weeks. We show that the frequency of sIPSCs
561 in layer II/III pyramidal cells of mPFC increases from neonatal to pre-juvenile period, consistent
562 with the developmental changes of IPSCs in layer III pyramidal neurons of monkey PFC
563 (González-Burgos et al. 2015) and mouse mPFC (Kroon et al. 2019).
564
565 **Pyramidal neurons and network activity**
566 It has been suggested that spontaneous network activity changes from local, highly synchronized
567 to more diffuse from the second to the third postnatal weeks, in the primary sensory cortices
568 (Golshani et al. 2009; Frye and MacLean 2016). Oscillatory activity in the mPFC first emerges at

P15 (Bitzenhofer et al. 2019). In this study, we have found increased spiking activity in the mPFC during the third, compared to the second postnatal week. This occurred despite the decreased excitatory and increased inhibitory synaptic function, but could be explained partly by the developmental increase of AP amplitude and rate of rise in the mPFC layer II/III pyramidal neurons, which could be due to the on-going maturation of sodium channels in pyramidal neurons.

Studies in developing mPFC pyramidal neurons have proposed that there is a unique sensitive time window for synaptic maturation of these neurons from individual cortical layers. During rat mPFC layer V development, the intrinsic properties, synaptic inputs and morphology of pyramidal neurons develop together during early postnatal life. While the greatest changes were reported during the first ten days after birth, the adult-like properties emerged after the end of the third week (P21) (Zhang et al. 2011). This study confirms that the second postnatal week is a period of rapid growth, similar to that in other neocortical regions by combining functional and structural measurements of developing pyramidal neurons in mouse mPFC (Zhu 2000; Romand et al. 2011).

Developmental PFC malformation leads to cognitive disorders in adulthood

The neonatal functional maturation of GABAergic circuits and E/I (excitation to inhibition) balance are critical for PFC-dependent behaviours and plasticity in the adult while their malfunction leads to many psychiatric disorders (Benes 1991; Kilb 2012; Ferguson and Gao 2018). From the prenatal period to late adolescence, the PFC network is highly vulnerable to genetic and environmental factors (Andersen 2003), since the mPFC is one of the latest cortical regions to develop (Huttenlocher 1990). While many studies have focused on understanding several developmental processes during adolescence (Caballero et al. 2016), our knowledge regarding the ongoing cellular and network developmental processes during the perinatal period is notably limited, despite significant evidence showing that environmental manipulations during this period manifest as complex psychiatric and neurologic disorders in adulthood (Weinberger 1986).

The delayed developmental shift of GABA action in various mouse models mimicking human brain disorders have been investigated, including the maternal immune activation model (Corradini et al. 2018; Fernandez et al. 2018), the Scn1a and Scn1b mouse models of Dravet syndrome (Yuan et al., 2019), the 22q11.2 deletion syndrome (Amin et al. 2017) and the Fmr1

deficient model of fragile X syndrome (He et al. 2018). In the latter study, early postnatal correction of GABA depolarization (bumetanide-treated) led to sufficient normalization of the mature BC network (He et al. 2018). The impaired KCC2 has been proposed as a potential therapeutic target of epilepsies by many studies in animal models and human patients (Moore et al. 2017).

Our study focuses in understanding the early developmental cellular and physiological mechanisms of mPFC circuits, before adolescence, and proposes that the neonatal mPFC compared to BC exhibits a delayed switch from depolarization to hyperpolarization function of $GABA_AR$. Our results raise the possibility that the delayed maturation of mPFC compared to other cortical areas depends on a combination of a delayed switch from depolarization to hyperpolarization function of the $GABA_AR$ and delayed maturation of interneurons.

Acknowledgements:

Authors are grateful to Emmanuella Foinikianaki for her help with Matlab analysis and histology and to Giasemi Eptaminitaki for her help in *in situ* hybridization experiments. They also would like to thank all the members of Karagogeos and Sidiropoulou Labs and the animal facility of the IMBB for help with experiments. This study was co-financed through the Operational Program "Education and Lifelong Learning" of the National Strategic Reference Framework – Research Funding Program (EDBM34) by a grant to DK (10040) and through the BIOIMAGING-GR, National Roadmap for Research Infrastructures from the European Union (European Social Fund-ESF) and Greek National Funds. KK has been a recipient of the Manasaki fellowship and a Medical School fellowship of the University of Crete and a poster award at the 27th Hellenic Society for Neuroscience Meeting.

Author Contributions:

All experiments were conceived and designed by K.K., K.S., and D.K. All experiments performed by K.K., A.V., O.C. and X.X. Data were analyzed by K.K., A.V., O.C., M.D. K.S. and discussed with D.K. X.X. and I.L.H.-O. X.X. carried out and analyzed the *in vivo* experiments. Manuscript was written by K.K., D.K. and K.S. All authors discussed and commented on the manuscript.

630 **References:**

631 Allene C, Cattani A, Ackman JB, Bonifazi P, Aniksztejn L, Ben-Ari Y, Cossart R. 2008. Sequential
632 Generation of Two Distinct Synapse-Driven Network Patterns in Developing Neocortex. J
633 Neurosci. 28:12851–12863.
634 Amin H, Marinaro F, De Pietri Tonelli D, Berdondini L. 2017. Developmental excitatory-to-
635 inhibitory GABA-polarity switch is disrupted in 22q11.2 deletion syndrome: a potential
636 target for clinical therapeutics. Scientific Reports. 1–18.
637 Andersen SL. 2003. Trajectories of brain development: point of vulnerability or window of
638 opportunity? Neuroscience & Biobehavioral Reviews. 27:3–18.
639 Bahrey HLP, Moody WJ. 2003. Early Development of Voltage-Gated Ion Currents and Firing
640 Properties in Neurons of the Mouse Cerebral Cortex. Journal of Neurophysiology. 89:1761–
641 1773.
642 Bartolini G, Ciceri G, Marin O. 2013. Integration of GABAergic Interneurons into Cortical Cell
643 Assemblies: Lessons from Embryos and Adults. 79:849–864.
644 Ben-Ari Y. 2001. Developing networks play a similar melody. Trends in Neurosciences. 24:353–
645 360.
646 Ben-Ari Y. 2002. Excitatory actions of gaba during development: the nature of the nurture. Nat
647 Rev Neurosci. 3:728–739.
648 Ben-Ari Y. 2012. Refuting the challenges of the developmental shift of polarity of GABA actions:
649 GABA more exciting than ever! 1–18.
650 Ben-Ari Y, Cherubini E, Corradetti R, Gaiarsa JL. 1989. Giant synaptic potentials in immature rat
651 CA3 hippocampal neurones. The Journal of Physiology. 416:303–325.
652 Ben-Ari Y, Gaiarsa JL, Tyzio R, Khazipov R. 2007. GABA: A Pioneer Transmitter That Excites
653 Immature Neurons and Generates Primitive Oscillations. Physiological Reviews. 87:1215–
654 1284.
655 Ben-Ari Y, Khalilov I, Kahle KT, Cherubini E. 2012. The GABA Excitatory/Inhibitory Shift in Brain
656 Maturation and Neurological Disorders. The Neuroscientist. 18:467–486.
657 Bendotti C, Hohmann C, Forloni G, Brain RRD, 1990. 1990. Developmental expression of
658 somatostatin in mouse brain. II. In situ hybridization. Elsevier. 53:26–39.
659 Benes FM. 1991. Deficits in Small Interneurons in Prefrontal and Cingulate Cortices of
660 Schizophrenic and Schizoaffective Patients. Archives of General Psychiatry. 48:996–1001.

661 Best JR, Miller PH. 2010. A Developmental Perspective on Executive Function. Child
662 Development. 81:1641–1660.
663 Bitzenhofer SH, Ahlbeck J, Wolff A, Wiegert JS, Gee CE, Oertner TG, Hanganu-Opatz IL. 2017.
664 Layer-specific optogenetic activation of pyramidal neurons causes beta-gamma entrainment
665 of neonatal networks. Nature Communications. 8:14563.
666 Bitzenhofer SH, Poepplau JA, Chini M, Marquardt A, Hanganu-Opatz I. 2019. Activity-dependent
667 maturation of prefrontal gamma oscillations sculpts cognitive performance. bioRxiv. 1–39.
668 Bitzenhofer SH, Sieben K, Siebert KD, Spehr M, Hanganu-Opatz IL. 2015. Oscillatory Activity in
669 Developing Prefrontal Networks Results from Theta-Gamma-Modulated Synaptic Inputs.
670 CellReports. 11:486–497.
671 Brockmann MD, Pöschel B, Cichon N, Hanganu-Opatz IL. 2011. Coupled Oscillations Mediate
672 Directed Interactions between Prefrontal Cortex and Hippocampus of the Neonatal Rat.
673 Neuron. 71:332–347.
674 Burgard EC, Hablitz JJ. 1993. Developmental changes in NMDA and non-NMDA receptor-
675 mediated synaptic potentials in rat neocortex. Journal of Neurophysiology. 69:230–240.
676 Caballero A, Flores-Barrera E, Cass DK, Tseng KY. 2014. Differential regulation of parvalbumin
677 and calretinin interneurons in the prefrontal cortex during adolescence. Brain Struct Funct.
678 219:395–406.
679 Caballero A, Granberg R, Tseng KY. 2016. Mechanisms contributing to prefrontal cortex
680 maturation during adolescence. Neuroscience & Biobehavioral Reviews. 1–29.
681 Casey BJ, Giedd JN, Thomas KM. 2000. Structural and functional brain development and its
682 relation to cognitive development. Biological Psychology. 54:241–257.
683 Chalkiadaki K, Velli A, Kyriazidis E, Stavroulaki V, Vouvoutsis V, Chatzaki E, Aivaliotis M,
684 Sidiropoulou K. 2019. Development of the MAM model of schizophrenia in mice: Sex
685 similarities and differences of hippocampal and prefrontal cortical function.
686 Neuropharmacology 144, 193–207.
687 Chini, M. & Hanganu-Opatz, I. L. 2020. Prefrontal Cortex Development in Health and Disease:
688 Lessons from Rodents and Humans. *Trends Neurosci*
689 Clancy B, Darlington RB, Neuroscience BF, 2001. 2001. Translating developmental time across
690 mammalian species. Elsevier. 105:7–17.
691 Corradini I, Focchi E, Rasile M, Morini R, Desiato G, Tomasoni R, Lizier M, Ghirardini E, Fesce R,
692 Morone D, Barajon I, Antonucci F, Pozzi D, Matteoli M. 2018. Maternal Immune Activation

693 Delays Excitatory-to-Inhibitory Gamma-Aminobutyric Acid Switch in Offspring. Biological
694 Psychiatry. 83:680–691.
695 de Lecea L, del Ri o JA, Soriano E. 1995. Developmental expression of parvalbumin mRNA in the
696 cerebral cortex and hippocampus of the rat. Molecular Brain Research. 32:1–13.
697 DeFelipe J, Fariñas I. 1992. The pyramidal neuron of the cerebral cortex: Morphological and
698 chemical characteristics of the synaptic inputs. Progress in Neurobiology. 39:563–607.
699 del Rio J, De Lecea L, Ferrer I, Soriano E. 1994. The development of parvalbumin-
700 immunoreactivity in the neocortex of the mouse. 81:247–259.
701 Del Rio JA, Soriano E, Ferrer I. 1992. Development of GABA-immunoreactivity in the neocortex
702 of the mouse. J Comp Neurol. 326:501–526.
703 Diamond A. 2005. Normal Development of Prefrontal Cortex from Birth to Young Adulthood:
704 Cognitive Functions, Anatomy, and Biochemistry. In: Principles of Frontal Lobe Function.
705 Oxford University Press. p. 466–503.
706 Doischer D, Aurel Hosp J, Yanagawa Y, Obata K, Jonas P, Vida I, Bartos M. 2008. Postnatal
707 Differentiation of Basket Cells from Slow to Fast Signaling Devices. J Neurosci. 28:12956–
708 12968.
709 Dzhala VI, Talos DM, Sdrulla DA, Brumback AC, Mathews GC, Benke TA, Delpire E, Jensen FE,
710 Staley KJ. 2005. NKCC1 transporter facilitates seizures in the developing brain. Nature
711 Medicine 2005 11:11. 11:1205–1213.
712 Ferguson BR, Gao W-J. 2018. PV Interneurons: Critical Regulators of E/I Balance for Prefrontal
713 Cortex-Dependent Behavior and Psychiatric Disorders. Front Neural Circuits. 12:479–13.
714 Fernandez A, Dumon C, Guimond D, Tyzio R, Bonifazi P, Lozovaya N, Burnashev N, Ferrari DC,
715 Ben-Ari Y. 2018. The GABA Developmental Shift Is Abolished by Maternal Immune Activation
716 Already at Birth. Cerebral Cortex. 130:e1447–11.
717 Fiumelli H, Cancedda L, Poo M-M. 2005. Modulation of GABAergic Transmission by Activity via
718 Postsynaptic Ca2+-Dependent Regulation of KCC2 Function. Neuron. 48:773–786.
719 Forloni G, Hohmann C, Research JCDB, 1990. 1990. Developmental expression of somatostatin
720 in mouse brain. I. Immunocytochemical studies. Elsevier. 53:6–25.
721 Frye CG, MacLean JN. 2016. Spontaneous activations follow a common developmental course
722 across primary sensory areas in mouse neocortex. Journal of Neurophysiology. 116:431–
723 437.
724 Fuster J. 2015. The Prefrontal Cortex. Academic Press.

725 Ganguly K, Schinder AF, Wong ST, Poo M-M. 2001. GABA Itself Promotes the Developmental
726 Switch of Neuronal GABAergic Responses from Excitation to Inhibition. Cell. 105:521–532.
727 Golshani P, Goncalves JT, Khoshkhoo S, Mostany R, Smirnakis S, Portera-Cailliau C. 2009.
728 Internally Mediated Developmental Desynchronization of Neocortical Network Activity. J
729 Neurosci. 29:10890–10899.
730 Gorin, M., C. Tsitoura, A. Kahan, K. Watznauer, D. R. Drose, M. Arts, R. Mathar, S. O'Connor, I. L.
731 Hanganu-Opatz, Y. Ben-Shaul and M. Spehr (2016). "Interdependent Conductances Drive
732 Infraslow Intrinsic Rhythmogenesis in a Subset of Accessory Olfactory Bulb Projection
733 Neurons." The Journal of Neuroscience 36(11): 3127-3144.
734 González-Burgos G, Miyamae T, Pafundo DE, Yoshino H, Rotaru DC, Hoftman G, Datta D, Zhang
735 Y, Hammond M, Sampson AR, Fish KN, Bard Ermentrout G, Lewis DA. 2015. Functional
736 Maturation of GABA Synapses During Postnatal Development of the Monkey Dorsolateral
737 Prefrontal Cortex. Cerebral Cortex. 25:4076–4093.
738 Gulledge AT, Stuart GJ. 2003. Excitatory Actions of GABA in the Cortex. Neuron. 37:299–309.
739 Guo ZV, Li N, Huber D, Ophir E, Gutnisky D, Ting JT, Feng G, Svoboda K. 2014. Flow of Cortical
740 Activity Underlying a Tactile Decision in Mice. Neuron. 81:179–194.
741 He Q, Arroyo ED, Smukowski SN, Xu J, Piochon C, Savas JN, Portera-Cailliau C, Contractor A. 2018.
742 Critical period inhibition of NKCC1 rectifies synapse plasticity in the somatosensory cortex
743 and restores adult tactile response maps in fragile X mice. Mol Psychiatry. 8:109–116.
744 Heidbreder CA, Groenewegen HJ. 2003. The medial prefrontal cortex in the rat: evidence for a
745 dorso-ventral distinction based upon functional and anatomical characteristics.
746 Neuroscience & Biobehavioral Reviews. 27:555–579.
747 Hensch TK. 2016. The Power of the Infant Brain. Nature Publishing Group. 314:64–69.
748 Huguenard JR, Hamill OP, Prince DA. 1988. Developmental changes in Na+ conductances in rat
749 neocortical neurons: appearance of a slowly inactivating component. Journal of
750 Neurophysiology. 59:778–795.
751 Huttenlocher PR. 1990. Morphometric study of human cerebral cortex development.
752 Neuropsychologia. 28:517–527.
753 Kaila K, Voipio J. 1987. Postsynaptic fall in intracellular p H induced by GABA-activated
754 bicarbonate conductance. Nature. 330:163–165.
755 Khazipov R, Luhmann HJ. 2006. Early patterns of electrical activity in the developing cerebral
756 cortex of humans and rodents. Trends in Neurosciences. 29:414–418.

Khazipov R, Minlebaev M, Valeeva G. 2013. Early gamma oscillations. Neuroscience. 250:240–252.

Khazipov R, Sirota A, Leinekugel X, Holmes GL, Ben-Ari Y, Buzsáki G. 2004. Early motor activity drives spindle bursts in the developing somatosensory cortex. Nature. 432:758–761.

Kilb W. 2012. Development of the GABAergic System from Birth to Adolescence. The Neuroscientist. 18:613–630.

Kirmse K, Kummer M, Kovalchuk Y, Witte OW, Garaschuk O, Holthoff K. 2015. GABA depolarizes immature neurons and inhibits network activity in the neonatal neocortex in vivo. Nature Communications. 6:7750.

Kolb B, Mychasiuk R, Muhammad A, Li Y, Frost DO, Gibb R. 2012. Experience and the developing prefrontal cortex. Proc Natl Acad Sci USA. 109:17186–17193.

Konstantoudaki X, Chalkiadaki K, Tivodar S, Karagogeos D, Sidiropoulou K. 2016. Impaired synaptic plasticity in the prefrontal cortex of mice with developmentally decreased number of interneurons. Neuroscience. 1–13.

Kriegstein AR, Suppes T, Prince DA. 1987. Cellular and synaptic physiology and epileptogenesis of developing rat neocortical neurons in vitro. Developmental Brain Research. 34:161–171.

Kroeze Y, Oti M, van Beusekom E, Cooijmans RHM, van Bokhoven H, Kolk SM, Homberg JR, Zhou H. 2017. Transcriptome Analysis Identifies Multifaceted Regulatory Mechanisms Dictating a Genetic Switch from Neuronal Network Establishment to Maintenance During Postnatal Prefrontal Cortex Development. Cerebral Cortex. 1–19.

Kroon T, van Hugte E, van Linge L, Mansvelder HD, Meredith RM. 2019. Early postnatal development of pyramidal neurons across layers of the mouse medial prefrontal cortex. Scientific Reports. 9:5037–16.

Le Magueresse C, Monyer H. 2013. GABAergic Interneurons Shape the Functional Maturation of the Cortex. Neuron. 77:388–405.

Liodis P, Denaxa M, Grigoriou M, Akufo-Addo C, Yanagawa Y, Pachnis V. 2007. Lhx6 Activity Is Required for the Normal Migration and Specification of Cortical Interneuron Subtypes. Journal of Neuroscience. 27:3078–3089.

LoTurco JJ, Owens DF, Heath MJS, Davis MBE, Kriegstein AR. 1995. GABA and glutamate depolarize cortical progenitor cells and inhibit DNA synthesis. Neuron. 15:1287–1298.

Lu J, Karadsheh M, Delpire E. 1999. Developmental regulation of the neuronal-specific isoform of K-CL cotransporter KCC2 in postnatal rat brains. J Neurobiol. 39:558–568.

789 Luhmann HJ, Prince DA. 1991. Postnatal maturation of the GABAergic system in rat neocortex.
790 Journal of Neurophysiology. 65:247–263.
791 Martina M, Royer S, Paré D. 2001. Cell-Type-Specific GABA Responses and Chloride Homeostasis
792 in the Cortex and Amygdala. Journal of Neurophysiology. 86:2887–2895.
793 McCormick DA, Prince DA. 1987. Post-natal development of electrophysiological properties of
794 rat cerebral cortical pyramidal neurones. The Journal of Physiology. 393:743–762.
795 Miyamae T, Chen K, Lewis DA, González-Burgos G. 2017. Distinct physiological maturation of
796 parvalbumin-positive neuron subtypes in mouse prefrontal cortex. J Neurosci. 3325–16–48.
797 Moore YE, Kelley MR, Brandon NJ, Deeb TZ, Moss SJ. 2017. Seizing Control of KCC2: A New
798 Therapeutic Target for Epilepsy. Trends in Neurosciences. 40:555–571.
799 Mòdol L, Bollmann Y, Tressard T, Baude A, Che A, Duan ZRS, Babij R, De Marco García NV, Cossart
800 R. 2019. Assemblies of Perisomatic GABAergic Neurons in the Developing Barrel Cortex.
801 Neuron. 1–18.
802 Owens DF, Boyce LH, Davis MBE, Kriegstein AR. 1996. Excitatory GABA Responses in Embryonic
803 and Neonatal Cortical Slices Demonstrated by Gramicidin Perforated-Patch Recordings and
804 Calcium Imaging. J Neurosci. 16:6414–6423.
805 Pan G, Yang J-M, Hu X-Y, Li X-M. 2017. Postnatal development of the electrophysiological
806 properties of somatostatin interneurons in the anterior cingulate cortex of mice. Nature
807 Publishing Group. 1–12.
808 Plotkin MD, Snyder EY, Hebert SC, Delpire E. 1997. Expression of the Na-K-2Cl cotransporter is
809 developmentally regulated in postnatal rat brains: A possible mechanism underlying GABA's
810 excitatory role in immature brain. J Neurobiol. 33:781–795.
811 Ramoa AS, McCormick DA. 1994. Developmental changes in electrophysiological properties of
812 LGNd neurons during reorganization of retinogeniculate connections. J Neurosci. 14:2089–
813 2097.
814 Rivera C, Voipio J, Payne JA, Ruusuvuori E, Lahtinen H, Lamsa K, Pirvola U, Saarma M, Kaila K.
815 1999. The K+/Cl- co-transporter KCC2 renders GABA hyperpolarizing during neuronal
816 maturation. Nature. 397:251–255.
817 Romand S, Wang Y, Toledo-Rodriguez M, Markram H. 2011. Morphological Development of
818 Thick-Tufted Layer V Pyramidal Cells in the Rat Somatosensory Cortex. Front Neuroanat. 5.
819 Rossant C, Kadir SN, Goodman DFM, et al. Spike sorting for large, dense electrode arrays. *Nat*
820 *Neurosci*. 2016;19(4):634-641. doi:10.1038/nn.4268

821 Schaeren-Wiemers N, Gerfin-Moser A. 1993. A single protocol to detect transcripts of various
822 types and expression levels in neural tissue and cultured cells: in situ hybridization using
823 digoxigenin-labelled cRNA probes. Histochemistry. 100:431–440.
824 Schubert D, Martens GJM, Kolk SM. 2014. Molecular underpinnings of prefrontal cortex
825 development in rodents provide insights into the etiology of neurodevelopmental disorders.
826 20:795–809.
827 Southwell DG, Paredes MF, Galvao RP, Jones DL, Froemke RC, Sebe JY, Alfaro-Cervello C, Tang Y,
828 García-Verdugo JM, Rubenstein JL, Baraban SC, Alvarez-Buylla A. 2012. Intrinsically
829 determined cell death of developing cortical interneurons. Nature. 491:109–113.
830 Spampanato J, Sullivan R. 2016. Development and physiology of GABAergic feedback excitation
831 in parvalbumin expressing interneurons of the mouse basolateral amygdala. Physiological
832 …. 4:e12664–15.
833 Tsujimoto S. 2008. The prefrontal cortex: functional neural development during early childhood.
834 The Neuroscientist. 14:345–358.
835 Van De Werd HJJM, Rajkowska G, Evers P, Uylings HBM. 2010. Cytoarchitectonic and
836 chemoarchitectonic characterization of the prefrontal cortical areas in the mouse. Brain
837 Struct Funct. 214:339–353.
838 Weinberger DR. 1986. Physiologic Dysfunction of Dorsolateral Prefrontal Cortex in
839 Schizophrenia. Archives of General Psychiatry. 43:114.
840 Yamada J, Okabe A, Toyoda H, Kilb W, Luhmann HJ, Fukuda A. 2004. Cl− uptake promoting
841 depolarizing GABA actions in immature rat neocortical neurones is mediated by NKCC1. The
842 Journal of Physiology. 557:829–841.
843 Yang JM, Zhang J, Yu YQ, Duan S, Li XM. 2013. Postnatal Development of 2 Microcircuits Involving
844 Fast-Spiking Interneurons in the Mouse Prefrontal Cortex. Cerebral Cortex. 24:98–109.
845 Yuan Y, Malley HAOX, Smaldino MA, Bouza AA, Hull JM, Isom LL. 2019. Delayed maturation of
846 GABAergic signaling in the Scn1a and Scn1b mouse models of Dravet Syndrome. Scientific
847 Reports. 1–16.
848 Zhang Z, Jiao Y-Y, Sun Q-Q. 2011. Developmental maturation of excitation and inhibition balance
849 in principal neurons across four layers of somatosensory cortex. Neuroscience. 174:10–25.
850 Zheng K, An JJ, Yang F, Xu W. 2011. TrkB signaling in parvalbumin-positive interneurons is critical
851 for gamma-band network synchronization in hippocampus. Proc Natl Acad Sci USA; 108
852 (41):17201-17206;

Zhu JJ. 2000. Maturation of layer 5 neocortical pyramidal neurons: amplifying salient layer 1 and layer 4 inputs by Ca2+ action potentials in adult rat tuft dendrites. The Journal of Physiology. 526:571–587.

Figures and figure legends

Figure 1

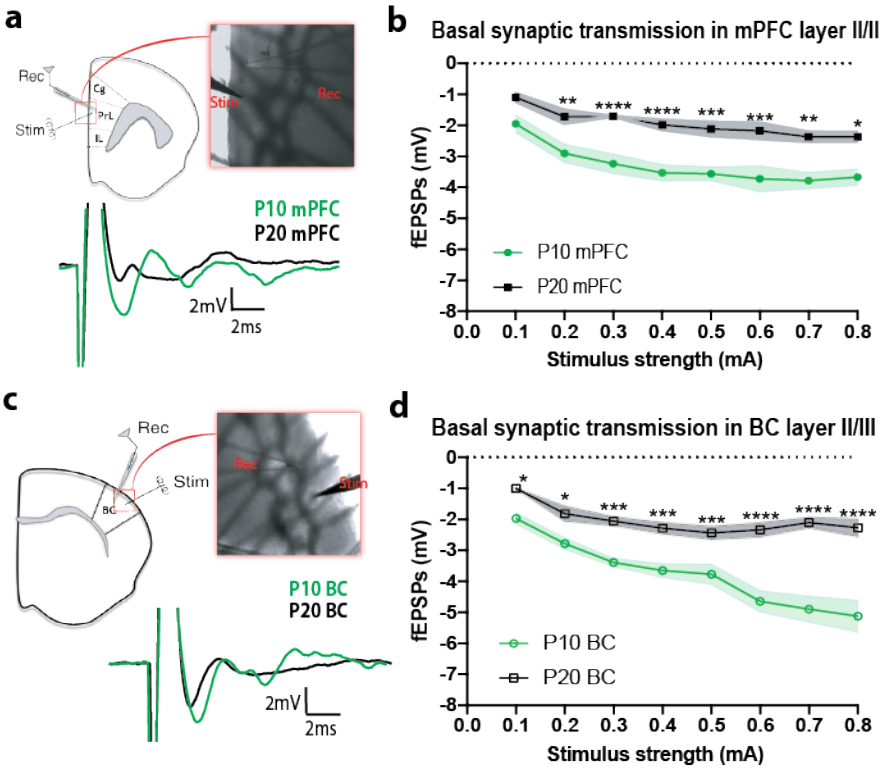

Figure 1. Basal Synaptic transmission is decreased in mPFC and BC across development

(**a, c**) (Top) Schematic representative photos showing the position of the electrodes in mPFC and BC brain slices (Rec: recording electrode, Stim: stimulating electrode). (Bottom) Representative traces showing the evoked field excitatory postsynaptic potentials (fEPSPs).

(**b,d**) Graphs showing the fEPSPs recorded in response to current pulses of increasing stimulus strength in layer II/III of mPFC (**b**) and BC (**d**). Two-way repeated measures ANOVA analyses of evoked fEPSPs revealed a significant effect of stimulus strength ($F_{(7, 82)}$ = 19.17, p<0.0001) and ages ($F_{(1, 82)}$ = 212.3, p<0.0001). Post-hoc analysis showed the fEPSPs significantly decreases at P20 compared to P10 in layer II/III of mPFC (Sidak's test, *p= 0.0106, **p=0.0012, ***p=0.0003 and ****p<0.0001) and BC (Sidak's test, *p=0.0279, ***p=0.0006 and ****p <0.0001), (n=6-7 brain slices from 3-4 WT male mice).

Figure 2

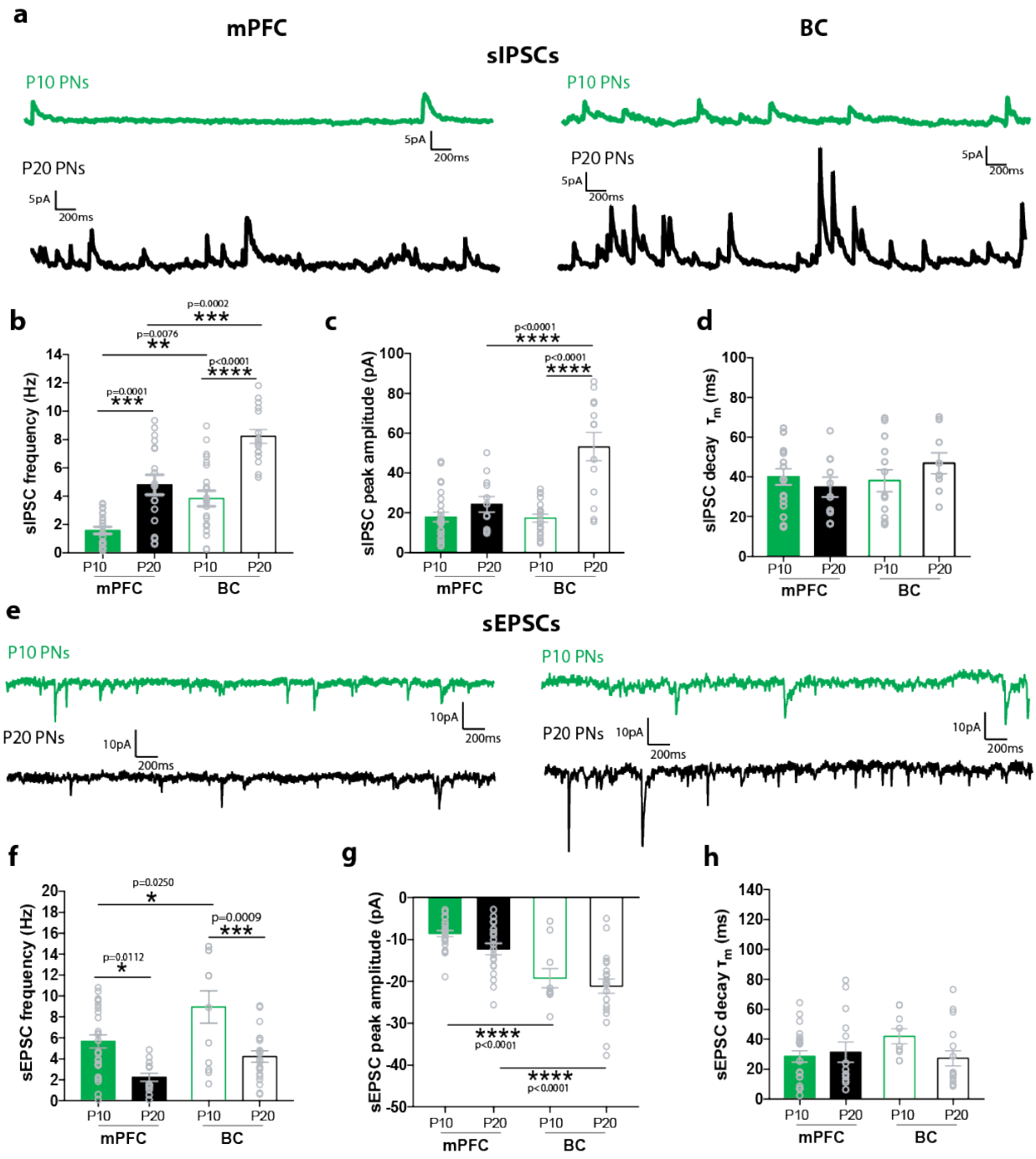

Figure 2. Properties of sIPSCs and sEPSCs at P10 and P20 of layer II/III mPFC and BC pyramidal neurons

(a) Representative traces of spontaneous inhibitory postsynaptic currents (sIPSCs) from layer II/III mPFC (left) and BC (right) pyramidal neurons at P10 (green) and P20 (black).

(b) Bar graph showing the sIPSC frequency (Hz) at P10 and P20 mPFC and BC pyramidal neurons. Two-way ANOVA analyses showed a significant effect of age ($F_{(1,74)}$=54.74, p<0.0001) and brain area ($F_{(1,74)}$=30.36, p<0.0001). Post-hoc analysis showed that sIPSC frequency was significantly

increased at P20 compared to P10 in mPFC (Tukey's test, p=0.0001) as well as in BC (p<0.0001). Furthermore, sIPSC frequency was significantly decreased in mPFC compared to BC at P10 (p=0.0076) as well as at P20 (p=0.0002).

(c) Bar graph showing the sIPSC peak amplitude at P10 and P20 of mPFC and BC pyramidal neurons. Two-way ANOVA analyses showed a significant effect of age ($F_{(1,65)}$=30.78, p<0.0001) and brain area (($F_{(1,65)}$=13.85 p<0.0001). Post-hoc analysis showed that the sIPSC amplitude (pA) was significantly increased at P20 compared to P10 in BC (p<0.0001) but not in mPFC (p=0.63). The sIPSC amplitude was significantly decreased at P20 in mPFC compared to BC (p<0.0001) but not at P10 between areas (p=0.9993).

(d) Bar graph showing the sIPSC decay time constant (τm) at P10 to P20 of mPFC and BC pyramidal neurons. Two-way ANOVA analyses did not show any significant effect of age ($F_{(1,45)}$=0.11, p=0.73) or brain area ($F_{(1, 45)}$=0.96, p=0.33) was found.

(e) Representative traces of spontaneous excitatory postsynaptic currents (sEPSCs) from layer II/III mPFC (left) and BC (right) pyramidal neurons at P10 (green) and P20 (black).

(f) Bar graph showing the sEPSC frequency at P10 to P20 of mPFC and BC pyramidal neurons. Two-way ANOVA analyses showed a significant effect of age ($F_{(1,68)}$=26.8, p<0.0001) and brain area ($F_{(1,68)}$=10,82, p=0.0016). Post-hoc analysis showed that the sEPSCs frequency significantly decreased at P20 compared to P10 in mPFC (p= 0.0112) and BC (p= 0.0009). Comparison of the two brain areas at P10, the sEPSCs frequency was significantly decreased in mPFC compared to BC (p= 0.0250).

(g) Bar graph showing the sEPSCs peak amplitude at P10 to P20 of mPFC and BC pyramidal neurons. Two-way ANOVA analyses showed a significant effect of brain area ($F_{(1,73)}$=42.7, p<0.0001) but not of age ($F_{(1,73)}$=3.435, p=0.067). The sEPSC amplitude was not significantly different at P10 and P20 in mPFC (p=0.1918) and BC (p=0.8617). On the other hand, the sEPSC amplitude was significantly decreased in mPFC compared to BC at P10 and P20 (p<0.0001).

(h) Bar graph showing the sEPSCs decay time constant (τm) at P10 to P20 of mPFC and BC pyramidal neurons. Two-way ANOVA analyses showed no significant effect of age ($F_{(1,57)}$=0.22, p=0.27) or brain area ($F_{(1,57)}$=0.77, p=0.39).

*All post-hoc tests values were based on Tukey's test; n=9-13 cells from 5-9 mice/age group.

Figure 3

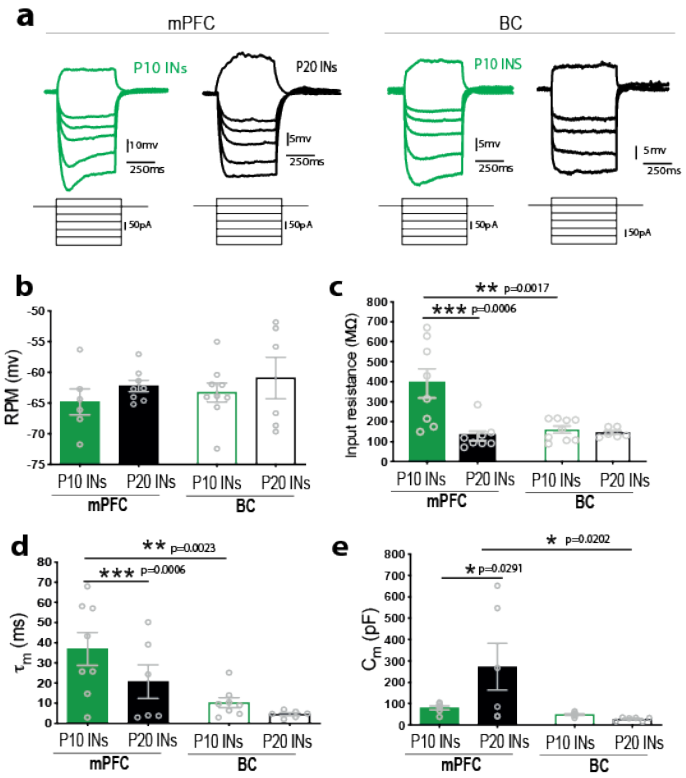

Figure 3. Passive membrane properties of Lhx6+ interneurons at P10 and P20 mPFC and P10 BC.

(a) Representative voltage responses (top traces) to 500ms positive and negative current pulses (bottom traces, +50, -50, -70, -100, -150, -200 pA) in mPFC at P10 and P20 and BC of Lhx6+ florescent interneurons from layer II/III.

(b) Bar graph showing the resting membrane potential (RMP) of interneurons at P10 and P20 in mPFC and BC. Two-way ANOVA analyses did not show any significant effect of age ($F_{(1,25)}$=1.55, p=0.22) or brain area ($F_{(1, 25)}$=0.50, p=0.48) was found., (n=6-9 cells from 5-6 mice/age group).

(c) Bar graph showing the input resistance of interneurons at P10 and P20 in mPFC and BC. Two-way ANOVA analyses showed a significant effect of age ($F_{(1,27)}$=10.94, p=0.0027) and brain area ($F_{(1,27)}$=6.65 p=0.0157). Post-hoc analysis showed that the input resistance significantly decreased at P20 compared to P10 in mPFC (Tukey's test, p=0.0006) and was significantly higher in mPFC compared with BC, at P10 (Tukey's test, p=0.0017), (n=8-9 cells from 5-6 mice/age group).

(d) Bar graph showing the membrane time constant (τ_m) of interneurons at P10 and P20 in mPFC and BC. Two-way ANOVA analyses showed a significant effect of age ($F_{(1,24)}$=14.71, p=0.0008) and brain area ($F_{(1,24)}$=6.92 p=0.0147). Post-hoc analysis showed that τ_m was

significantly higher at P10 compared to P20 in mPFC (Tukey's test, p=0.0006) while it was significantly higher in mPFC compared to BC, at P10 (Tukey's test, p=0.0023), (n=8-9 cells from 5-6 mice/age group).

(e) Bar graph showing the membrane capacitance (C_m) of interneurons at P10 and P20 in mPFC and BC. Two-way ANOVA analyses showed a significant effect between brain areas ($F_{(1,21)}$=6.82, p=0.00163) and not between ages ($F_{(1,21)}$=2.60 p=0.1219). Post-hoc analysis showed that Cm was significantly higher at P10 compared with P20 in mPFC (Tukey's test, p=0.0291) and was not significantly different between mPFC and BC, at P10 (Tukey test, p=0.97) while it was significantly higher at P20 in mPFC compared to P20 in BC (Tukey test, p=0.0202), (n=6-9 cells from 5-6 mice/age group).

Figure 4

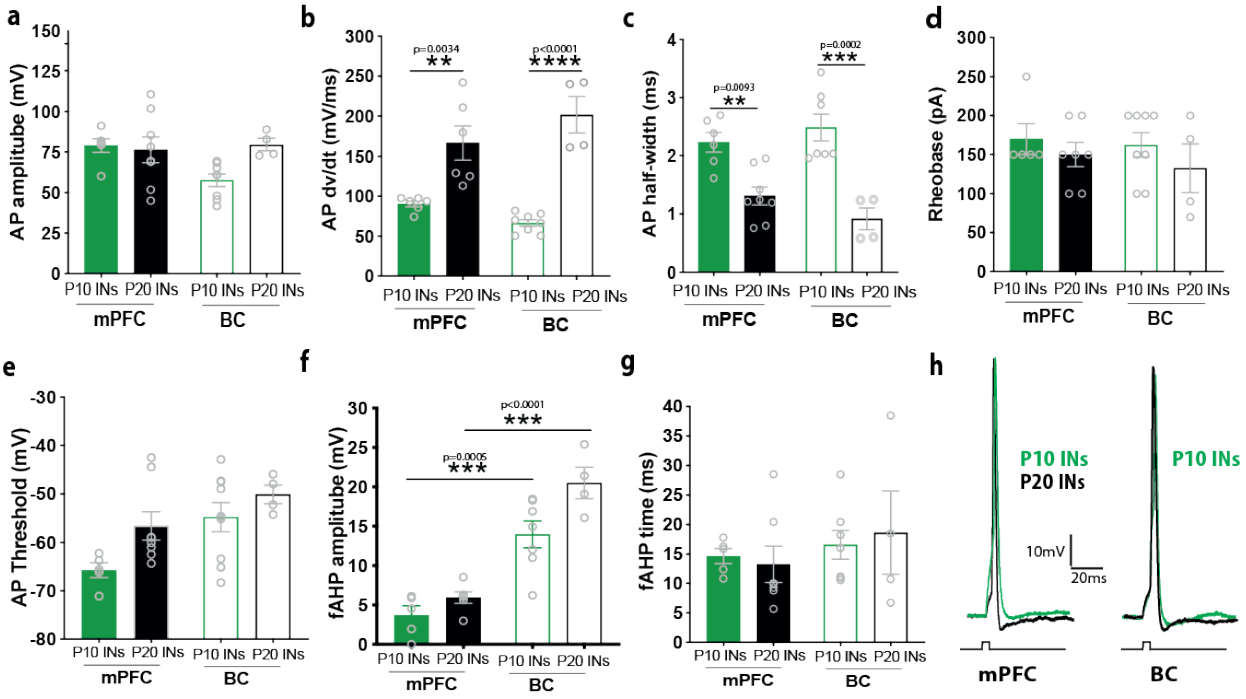

Figure 4. Poor development of active membrane properties of Lhx6^{+} interneurons in mPFC.

(a) Bar graph showing the action potential (AP) amplitude of interneurons at P10 and P20 in mPFC and BC. Two-way ANOVA analyses did not show any significant effect of age ($F_{(1,22)}$=2.46, p=0.13) or brain area ($F_{(1, 22)}$=2.13, p=0.15) was found., (n=6-9 cells from 5-6 mice/age group).

(b) Bar graph showing the AP rate of rise (dv/dt) of interneurons at P10 and P20 in mPFC and at P10 in BC. Two-way ANOVA analyses showed a significant effect between ages ($F_{(1,20)}$=58.96, p<0.0001) but not brain area ($F_{(1,20)}$=0.16 p=0.69). Post-hoc analysis showed that the AP rate of rise significantly increased at P20 compared to P10 in mPFC (Tukey's test, p=0.0034) and at P20 compared to P10 in BC (Tukey's test, p<0.001), (n=6-9 cells from 5-6 mice/age group).

(c) Bar graph showing the AP duration (half-width) of interneurons at P10 and P20 in mPFC and BC. Two-way ANOVA analyses showed a significant effect between ages ($F_{(1,21)}$=39.16, p<0.0001) but not brain area ($F_{(1,21)}$=0.16 p=0.73). Post-hoc analysis showed that the AP duration significantly decreased at P20 compared to P10 in mPFC (Tukey's test, p= 0.0093) and at P20 compared to P10 in BC (Tukey's test, p=0.0002), (n=6-9 cells from 5-6 mice/age group).

(d) Bar graph showing the AP rheobase of interneurons at P10 and P20 in mPFC and BC. Two-way ANOVA analyses did not show any significant effect of age ($F_{(1,20)}$=1.60, p=0.22) or brain area ($F_{(1, 20)}$=0.40, p=0.53) was found.

(e) Bar graph showing the AP threshold of interneurons at P10 and P20 in mPFC and BC. . Two-way ANOVA analyses showed significant effect of age ($F_{(1,22)}$=5.048, p=0.035) and brain area ($F_{(1, 22)}$=8.00, p=0.009) was found. Post-hoc analysis showed that the AP threshold was not significantly different at P20 compared to P10 in mPFC (Tukey's test, p=0.1673) and in BC (Tukey's test, p=0.72009) or at P10 in mPFC compared to P10 in BC (Tukey's test, p=0.067) and at P20 in mPFC compared to P20 in BC (Tukey's test, p=0.72).

(f) Bar graph showing the AHP (afterhypolarization) amplitude of interneurons at P10 and P20 in mPFC and BC. Two-way ANOVA analyses showed significant effect of age ($F_{(1,18)}$=7.35, p=0.0143) and brain area ($F_{(1, 18)}$=63.72, p<0.0001) was found. Post-hoc analysis showed that the AHP amplitude was not significantly different at P20 compared to P10 in mPFC (Tukey's test, p=0.7187) and was significantly decreased in mPFC compered to BC, at P10 (Tukey's test, p= 0.0005) and in mPFC compered to BC at P20 (Tukey's test, p<0.00001), (n=6-9 cells from 5-6 mice/age group).

(g) Bar graph showing the AHP time of interneurons at P10 and P20 in mPFC and BC. Two-way ANOVA analyses did not show any significant effect of age ($F_{(1,19)}$=0.009, p=0.92) or brain area ($F_{(1, 19)}$=1.074, p=0.31) was found.

(h) Representative traces of APs of layer II/III Lhx6+ interneurons in mPFC (left) and BC (right) at P10 (green) and P20 (black).

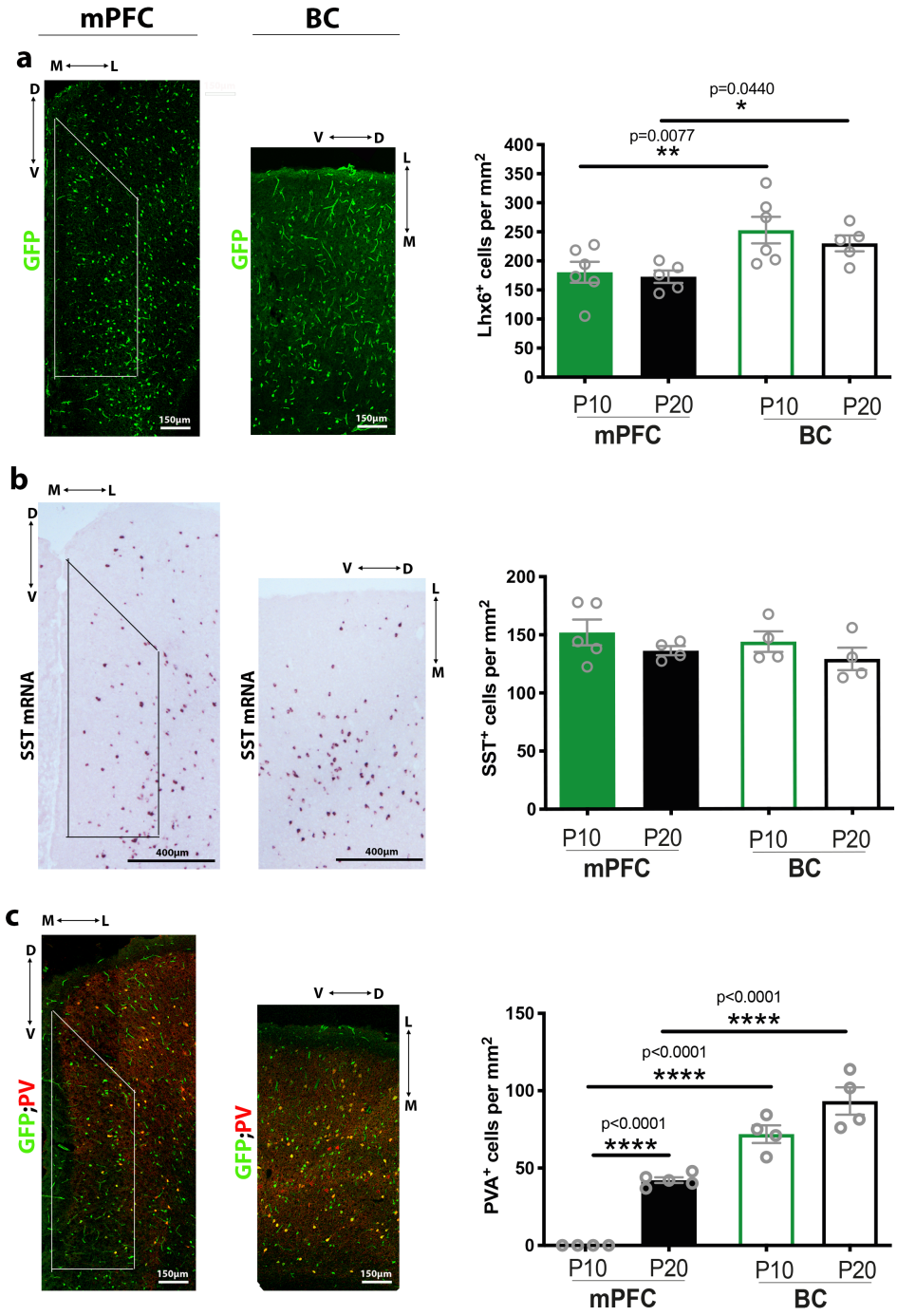

Figure 5. Significant differences in cellular density of Lhx6⁺ interneurons in mPFC and BC at P10 and P20.

(a) A representative immunostaining with GFP for Lhx6⁺ interneurons in Lhx6-cre;ROSA26fl-STOPfl-YFP mice in mPFC and BC at P20 is showing on the left. Scale bars: 150 µm. On the right, bar graph comparing Lhx6⁺ interneurons cell density (per mm^2) at P10 and P20 in mPFC and BC. Two-way ANOVA analyses of the cell density revealed a significant effect of brain area ($F_{(1, 18)}$ =

13.11, p=0.0020), but not of age ($F_{(1,18)}$=0.7185, p=0.4078). Post-hoc analysis showed that the Lhx6$^+$ cell density was not significant different at P20 compared to P10 in mPFC and BC (LSD test, p=0.77 and p= 0.38, respectively). The Lhx6$^+$ cell density was significantly lower in mPFC compared to BC at P10 and P20, respectively (LSD test, p=0.0077 and p= 0.0440, respectively), (P10 in mPFC and BC:n= 5 mice, P20 in mPFC and BC: n=4).

(b) A representative in situ hybridization staining for somatostatin positive cells (SST$^+$) using wild type animals in mPFC and BC at P20 is showing on the left. Scale bar: 200µm. Bar graph comparing cell density based on SST$^+$ expression at P10 and P20 in mPFC and BC. Two-way ANOVA analyses of the cell density showed no significant effect of age ($F_{(1, 13)}$= 2.78, p=0.12) and brain area ($F_{(1,13)}$=071, p=0.41) was found, (P10 in mPFC: n= 5 mice, P10 in BC and P20 in mPFC and BC: n=4).

(c) A representative double immunostaining for GFP; PV (PV: parvalbumin) in mPFC and BC at P20 is showing on the left. Scale bars: 150 µm. On the right, bar graph comparing cell density based on PV$^+$ expression at P10 and P20 in mPFC and BC. Two-way ANOVA analyses of the cell density revealed a significant effect of age ($F_{(1, 14)}$ = 45.49, p<0.0001) and brain area ($F_{(1, 14)}$ = 170.2, p<0.0001). PV$^+$ cells were not found in mPFC but were identified in BC, at P10. Post-hoc analysis showed that the PV$^+$ cell density was not significantly different at P20 compared to P10 in BC (LSD test, p= 0.1089), but was significantly lower in mPFC compared to BC at P20 (LSD test, p<0.0001), (P10 and P20 in mPFC: n= 5 mice, P10 and P20 in BC: n=4).

Figure 6

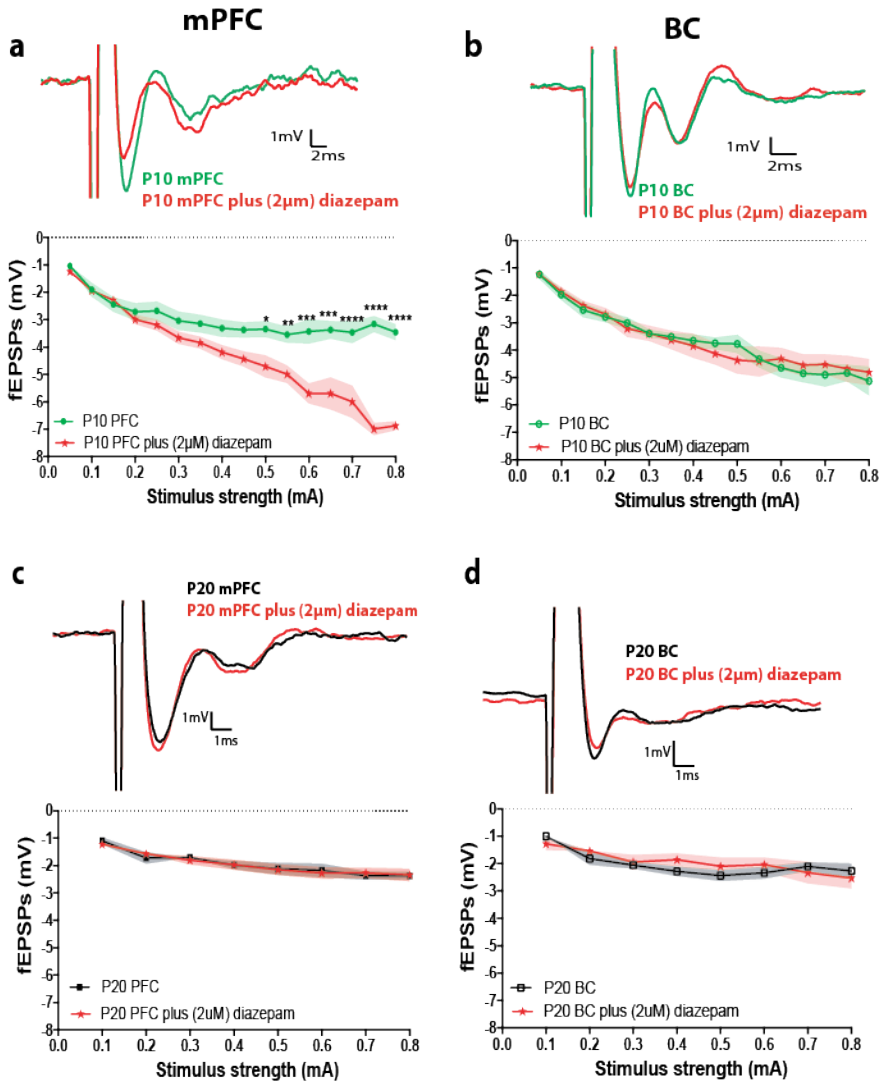

Figure 6. Increased $GABA_AR$ activity leads to enhanced fEPSPs in mPFC during the second postnatal week.

fEPSPs were recorded were recorded in layer II/III in response to current pulses of increasing stimulus strength of layer II/III, during two experimental treatments, before and after application of 2µM diazepam ($GABA_AR$ agonist) at P10 and P20 of mPFC and BC in mice.

(a) Representative traces (left) and graph (right) showing the fEPSPs amplitude before (green) and after (red) diazepam bath application, in mPFC at P10. Two-way repeated measures ANOVA analyses of evoked fEPSPs revealed significant effect of stimulus strength ($F_{(15,135)}$ = 25.64, p<0.0001) and experimental treatments ($F_{(1, 135)}$ = 136.1, p<0.0001). Post-hoc analysis showed that the fEPSP amplitude significantly increased in mPFC at P10 after diazepam bath application

(Sidak's test, *p= 0.0175, **p=0.0082, ***p=0.0002 and ****p<0.0001 at 0.3, 0.4. 0.5, 0.6 and 0.7 mA respectively), (n=6-7 brain slices from 3-4 mice).

(b) Graph (right) and representative traces (left) showing that diazepam bath application does not have any effect on the fEPSP amplitude in BC at P10. Two-way repeated measures ANOVA analyses of evoked fEPSPs revealed a significant effect of stimulus strength ($F_{(15, 140)} = 24.05$, $p<0.0001$) but not experimental conditions ($F_{(1, 135)} = 0.03$, $p=0.86$), (n=6-7 brain slices from 3-4 mice).

(c) Graph (right) and representative traces (left) showing that diazepam bath application does not have any effect on the fEPSP amplitude in mPFC at P20. Two-way repeated measures ANOVA analyses of evoked fEPSPs revealed a significant effect of stimulus strength ($F_{(7, 96)} = 10.36$, $p<0.0001$) but not experimental conditions ($F_{(1,96)}=0.03$, $p=0.9382$), (n=6-7 brain slices from 3-4 mice).

(d) Graph (right) and representative traces (left) showing that bath application of diazepam does not have any effect in the fEPSP amplitude in BC at P20. Two-way repeated measures ANOVA analyses of evoked fEPSPs revealed a significant effect of stimulus strength ($F_{(7, 96)} = 5.51$, $p<0.0001$) but not experimental conditions ($F_{(1, 96)} = 0.50$, $p=0.47$), (n=6-7 brain slices from 3-4 mice).

Figure 7

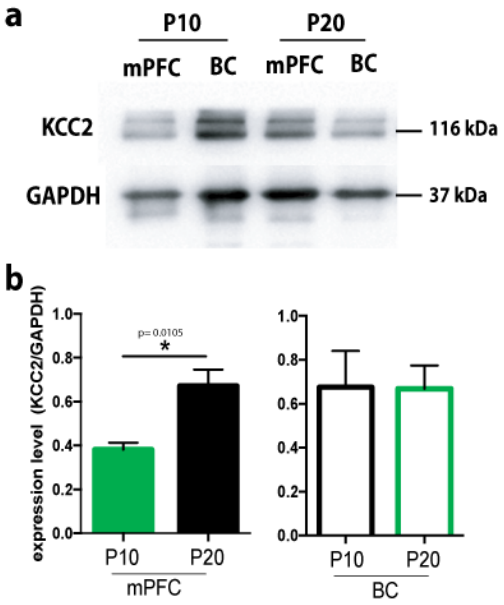

Figure 7. Decreased levels of K+-Cl- co-transporter 2 (KCC2) in mPFC during the second postnatal week.

(a) Representative blots showing changes of the K-Cl co-transporter (KCC2) levels, relative to GAPDH at P10 and P20 in mPFC and BC.

(b) Graph showing the normalized protein level (KCC2/GAPDH) in mPFC and BC at P10 and P20. The KCC2 protein levels was significantly increased at P20 compared to P10 in mPFC (two-tailed t-test, p= 0.01) but not in BC (two-tailed t-test, p= 0.97) (n=3-4 mice).

Figure 8

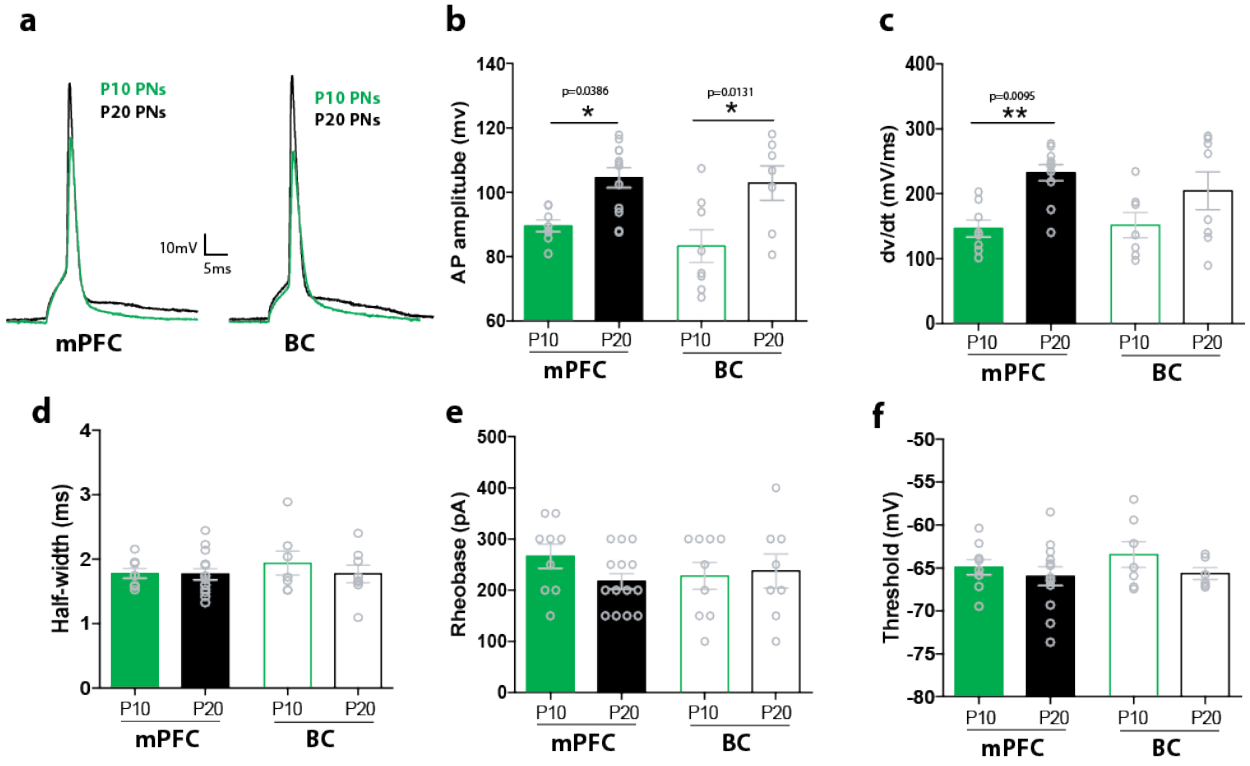

Figure 8. Active properties of mPFC and BC pyramidal neurons.

(a) Representative traces of action potentials (APs) of layer II/III pyramidal neurons in mPFC (left) and BC (right) at P10 (green) and P20 (black), respectively.

(b) Bar graph showing the AP amplitude of pyramidal neurons at P10 and P20 in mPFC and BC. Two-way ANOVA analyses showed a significant effect of age ($F_{(1, 31)}$ = 18.74, p=0.0001) but not on brain area ($F_{(1, 31)}$ = 0.99, p=0.32) was found. Post-hoc analysis showed that the AP amplitude significantly increased at P20 compared to P10 in mPFC and BC (Tukey's test, p=0.0386 and p= 0.0131, respectively) (n=9-14 cells from 6-10 mice/age group).

(c) Bar graph showing the AP rate of rise (dv/dt) of pyramidal neuron at P10 and P20 in mPFC and BC. Two-way ANOVA analyses showed a significant effect of age ($F_{(1,30)}$= 13.53, p=0.0009) but not on brain area ($F_{(1, 30)}$ = 0.36, p=0.55) was found. Post-hoc analysis showed that the AP rate of rise significantly increased at P20 compared to P10 in mPFC (Tukey's test, p= 0.0095), but not in BC (Tukey's test, p= 0.25) (n=8-14 cells from 6-10 mice/age group).

(d) Bar graph showing the AP duration (half-width) of pyramidal neuron at P10 and P20 in mPFC and BC. Two-way ANOVA analyses showed no significant effect of age (F(1, 33) = 0.52, p=0.47) or brain area ($F_{(1, 33)}$ = 0.43, p=0.51) was found (n=9-14 cells from 6-10 mice/age group).

(e) Bar graph showing the AP rheobase of pyramidal neuron at P10 and P20 in mPFC and BC. Two-way ANOVA analyses showed no significant effect of age ($F_{(1, 36)}$ = 0.66, p=0.41) or brain area ($F_{(1, 36)}$ = 0.16, p=0.69) was found (n=9-14 cells from 6-10 mice/age group).

(f) Bar graph showing the AP threshold of pyramidal neuron at P10 and P20 in mPFC and BC. Two-way ANOVA analyses showed no significant effect of age ($F_{(1,31)}$ = 1.90, p=0.17) or brain area ($F_{(1,31)}$=0.55, p=0.46) was found (n=9-14 cells from 6-10 mice/age group).

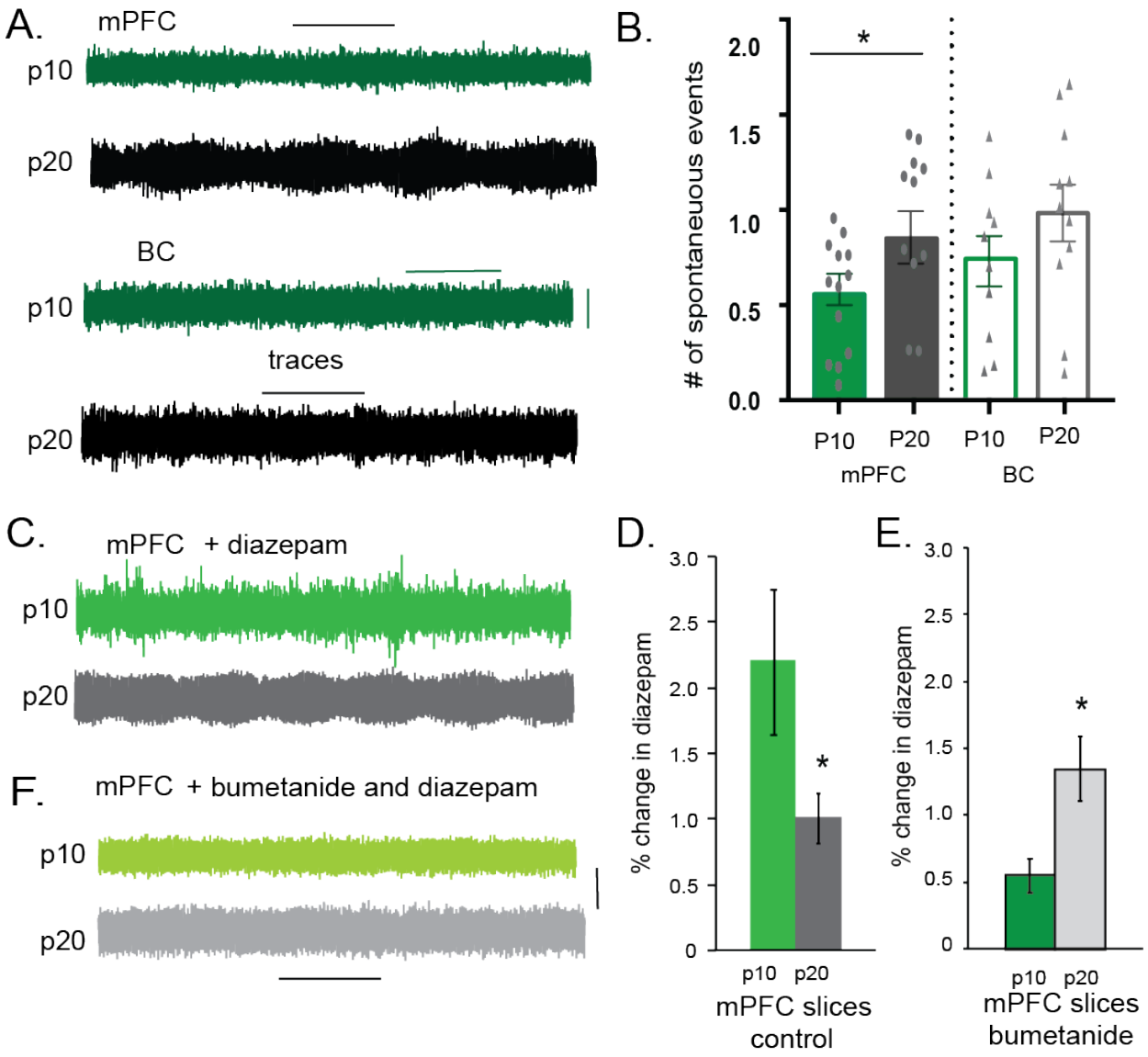

Figure 9. Spontaneous activity events in mPFC and BC brain slices.

(a) Representative traces of spontaneous activity in mPFC and BC brain slices at P10 and P20.

(b) Graph showing that the number of spontaneous activity events in mPFC and BC brain slices at P10 and P20. Two-way ANOVA analyses showed a significant effect of age ($F_{(1,32)}$= 11.48, p=0.0016) but not on brain area ($F_{(1, 39)}$ = 0.09, p=0.77) was found. The number of spontaneous events was significantly increased in the mPFC at P20 compared to P10 (Sidak's test, p= 0.0132), but in BC at P20 compared to P10 (Sidak's test, p= 0.5851)._

(c) Representative traces of spontaneous activity in mPFC following the addition of diazepam and diazepam + bumetanide at P10 and P20.

(d) Graph showing that the percent change due to diazepam is significantly increased at P10, compared to P20 (t-test, p=0.02).

(e) Graph showing that the percent change due to diazepam, in the presence of bumetanide, is significantly reduced at P10, compared to P20 (t-test, p=0.03).

Figure 10

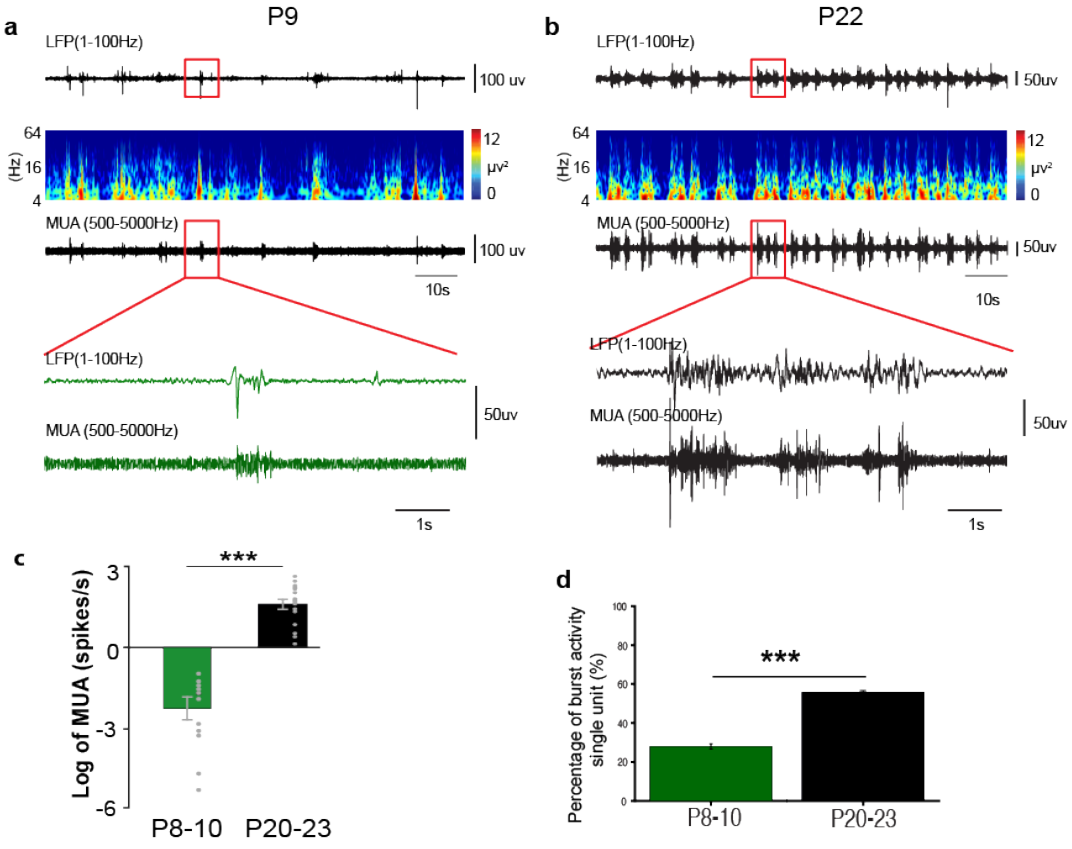

Figure 10. Spike activity in PFC of neonatal and pre-juvenile mice.

(a) Extracellular LFP recordings of oscillatory activity in PFC from a P9 mouse displayed after bandpass (1-100 Hz) filtering (top) and the corresponding MUA after bandpass (500-5000 Hz) filtering (bottom). Traces are accompanied by the color-coded wavelet spectra of the LFP at identical time scale.

(b) the same display as (**a**), but in one P22 mouse.

(c) Bar diagram displaying the mean MUA of neurons in PFC of neonatal and pre-juvenile mice. During development, significant increase of MUA in PFC in pre-juvenile mice (n=14) compared with in neonatal mice (n=13) (1.71±0.16 vs. -2.29±0.45, $p<0.0001$, One-way ANOVA, $F_{(1, 25)}=80.19$).

(d) Bar diagram displaying the percentage of the burst activity of single units in PFC of neonatal and pre-juvenile mice. During development, significant more burst activity per single unit in PFC in pre-juvenile mice (150 single unit) than in neonatal mice (161 single unit) (55.73±0.92 % vs. 27.90±1.41 %, $p<0.0001$, One-way ANOVA, $F(1, 309)=272.26$). In neonatal mice, 21 out 161 single

1255 units were classified as “burst unit”. In pre-juvenile mice, 104 out of 150 single units were
1256 classified as “burst unit”.
1257